Simulation of the Tropical Climate of an Ice Age

SYUKURO MANABE AND DOUGLAS G. HAHN

Geophysical Fluid Dynamics Laboratory/NOAA, Princeton University
Princeton, New Jersey 08540

Numerical time integrations of a general circulation model of the atmosphere are performed with both modern and ice age boundary conditions. It is shown that the climate of continental portions of the tropics in the ice age simulation is much drier than that of the modern climate simulation. According to comparisons of results from the two experiments, tropical continental aridity of the ice age results from stronger surface outflow from (or weaker surface inflow into) continents. The intensification of outflow from (or weakening of inflow into) tropical continental regions results from the fact that in response to ice age boundary conditions, atmospheric temperature is reduced more over continents than over oceans. With the exception of high latitudes, boundary condition differences between the two experiments consist mainly of changes of the prescribed values of sea surface temperature and continental albedo. In order to evaluate the relative contributions of these changes in producing continental tropical aridity in the ice age simulation, a third numerical experiment is time-integrated in which a hybrid combination of ice age sea surface temperatures and modern continental albedo values is prescribed. From intercomparisons between results from this and the previous two experiments it is shown that the effect of increased continental albedo is mainly responsible for the weak Asian monsoon in the ice age simulation.

INTRODUCTION

During the past 20 years, mathematical models of the atmosphere have improved sufficiently to simulate many of the geographical features of climate. Therefore it is quite reasonable to consider the possibility of using such a model for the study of an ice age climate. This is one of the important reasons why a large group of geologists [i.e., *Climap Project Members,* 1976] have embarked upon an ambitious project aiming at the reconstruction of conditions at the earth's surface (i.e., sea surface temperature, glacial ice, surface albedo, etc.) during the period of the last glacial maximum, which occurred approximately 18,000 yr B.P. This paper discusses a part of the results from a numerical simulation with a global model of the atmosphere in which geological reconstructions made by Climate: Long-Range Investigation Mapping and Prediction (Climap) are used as lower boundary conditions. It is expected that the combined effort of geological reconstruction and mathematical simulation will yield a comprehensive picture of an ice age climate. In addition, by comparing the simulated ice age climate with a simulation of the present climate, one may obtain an appreciation of the circumstances under which an ice age climate is maintained. Furthermore, such comparisons may yield some insight into how climate (or atmospheric circulation) responds to anomalies in the lower boundary conditions, i.e., anomalies in the distributions of sea surface temperature, surface albedo, and glacial ice.

It should be pointed out that this is not the first attempt to simulate an ice age climate. Earlier attempts of a similar nature include works by *Alyea* [1972], *Williams et al.* [1974], *Saltzman and Venekar* [1975], and *Gates* [1976*a, b*]. In particular, Gates conducted a numerical integration of a global model using Climap boundary conditions which are very similar to those used for the present study. Nevertheless, it was decided to carry out a similar numerical integration using a model developed at the Geophysical Fluid Dynamics Laboratory of NOAA in view of its success in simulating modern distributions of hydrologic quantities (i.e., precipitation and evaporation), particularly in the tropics [*Manabe and Holloway,* 1975]. Instead of discussing every aspect of the results from this ice age simulation it was therefore decided to place the main emphasis of this study upon the analysis of the simulated climate and the hydrologic cycle in the tropics.

Earlier literature [e.g., *Charlesworth,* 1957] suggests that in the tropics the climate of a glacial period is more pluvial than that of an interglacial period. One may speculate that the meridional temperature gradient during a glacial period is larger than that of an interglacial period owing partly to the large reflectivity of the extensive ice sheets in high latitudes. Therefore it may not be unreasonable to expect stronger Hadley cells and, accordingly, more intense tropical precipitation during a glacial period. However, more recent geological evidence [e.g., *Williams,* 1975] indicates that many parts of tropical continents were more arid during the late Pleistocene, in apparent contrast to the earlier notion of pluvial tropics during glacial periods. This paper describes the aridity (or lack of aridity) of the tropical climate of the model, evaluates the two contradictory viewpoints in the light of results from the numerical experiments, and proceeds to discuss how the lower boundary conditions of an ice age influence the climate and, in particular, the hydrologic cycle in the tropics.

Before this introductory section is concluded, it should be noted that this study does not attempt to simulate the seasonal variation of an ice age climate. Instead, it was decided to limit the scope of this study to the simulation of only one season (July-August) pending completion of the reconstruction of the January-February boundary conditions by the Climap group. Nevertheless, the results from this study appear to be very useful for identifying the important mechanisms which control the aridity of tropical continents. Therefore it was decided to write this paper despite the highly preliminary nature of the results. Future plans include the time integration of a model with ice age boundary conditions for an extended period of more than 1 year.

DESCRIPTION OF THE MODEL

The numerical model used in this study is identical to the one described by *Manabe et al.* [1974]. The details of the model structure are described by *Holloway and Manabe* [1971]. Therefore only a brief description of the model is given here.

The model performs the time integration of the primitive equations of motion in a spherical coordinate system. The dynamical effect of mountains is taken into consideration by

Paper number 7C0357.

TABLE 1. Boundary Conditions of the Standard, SST, and Ice Age Experiments

Experiment	Sea Surface Temperatures	Albedo	Topography, Continental Outlines, and Earth's Orbital Parameters
Standard	present	present	present
SST	18,000 yr B.P.	present	present
Ice age	18,000 yr B.P.	18,000 yr B.P.	18,000 yr B.P.

using the sigma coordinate system in which pressure normalized by surface pressure is the vertical coordinate [*Phillips*, 1957]. The effects of subgrid scale mixing are represented by the nonlinear viscosity formulated by *Smagorinsky* [1963]. The finite difference forms of the dynamical equations are similar to those proposed by *Kurihara and Holloway* [1967]. The global grid system is chosen such that the horizontal grid size of approximately 265 km is as uniform as possible. The 11 vertical finite difference levels are selected so that the model is able to crudely simulate the structure of the stratosphere as well as the planetary boundary layer. (See Table 1 of *Manabe et al.* [1974] for details.)

The scheme for computing radiative heating and cooling is described by *Manabe and Strickler* [1964] and *Manabe and Wetherald* [1967]. The solar radiation at the top of the atmosphere is a function of both latitude and season, but its diurnal variation is eliminated for simplicity. The seasonal variation of insolation is controlled by changes in both solar declination and distance, which are functions of the date. The depletion of solar radiation and the transfer of terrestrial radiation are computed by taking into consideration clouds, water vapor, carbon dioxide, and ozone distributions. An annual mean observed distribution of clouds, which varies with latitude and height but not with longitude, is used in the computation of radiative transfer. The distribution of water vapor is determined by the prognostic equations of the model. An observed distribution of ozone is prescribed as a function of season, latitude, and height. The mixing ratio of carbon dioxide by weight is assumed to have a constant value of 0.456×10^{-3} everywhere. For the computation of reflected solar radiation a geographical distribution of surface albedo is prescribed over continents. However, when snow accumulation is predicted on the ground surface, the base albedo is replaced by a higher albedo of snow cover as computed from equations (11) and (12) of *Holloway and Manabe* [1971].

The surface temperature over land is determined by the boundary condition that no heat is stored in the ground, i.e., net fluxes of solar and terrestrial radiation and turbulent fluxes of sensible and latent heat locally add to zero. Over the oceanic part of the model the seasonal variation of surface temperature is prescribed. The surface temperature of sea ice is computed in a manner similar to the computation of land surface temperature except that heat conduction through ice is taken into consideration. For the sake of simplicity, it is assumed that sea ice has a uniform thickness of 2 m. The seasonal variation of the area covered by sea ice is prescribed.

The prognostic system of water vapor consists mainly of the contributions by the three-dimensional advection of water vapor, evaporation from the earth's surface, vertical mixing of water vapor in the planetary boundary layer, nonconvective condensation, and a so-called 'moist convective adjustment.' For a more specific description of moist adjustment, see *Manabe et al.* [1965].

The schemes for computing the hydrology of the ground surface are similar to those described by *Manabe* [1969*a*]. The rates of change of soil moisture and snow depth are determined by the budget of water, snow, and heat at the ground surface.

DESIGN OF EXPERIMENTS

From the general circulation model described in the preceding section, three numerical experiments are conducted using the three different sets of boundary conditions indicated in Table 1. The first experiment, which is called the standard experiment, attempts to simulate the present climate. The boundary conditions adopted for this experiment are seasonally varying distributions of observed sea surface temperature and sea ice, solar radiation at the top of the atmosphere as determined from modern values of the earth's orbital parameters, a smoothed distribution of present topography, and a base albedo field as determined by *Posey and Clapp* [1964]. This model is integrated for 3.5 model years, as is indicated in Figure 1. Further details of the boundary conditions and the results from this experiment were extensively discussed by *Manabe and Holloway* [1975], *Manabe et al.* [1974], *Hahn and Manabe* [1975], and *Manabe and Mahlman* [1976].

The second experiment, which is called the ice age experiment, attempts to simulate an ice age climate. As Figure 1 indicates, the initial condition for this time integration is the state of the model atmosphere on April 20 in the last year of integration of the standard experiment. This integration is continued for a period of 134 model days and is terminated on September 1. The solar radiation at the top of the model atmosphere is computed from the values of orbital parameters computed for 18,000 yr B.P. The distribution of seasonally varying sea surface temperature is determined by adding the following quantity to the modern seasonally varying sea surface temperature distribution: $T_s^{\text{Aug}}(18{,}000 \text{ yr B.P.}) - T_s^{\text{Aug}}(P)$, where $T_s^{\text{Aug}}(18{,}000 \text{ yr B.P.})$ and $T_s^{\text{Aug}}(P)$ are the Climap and modern distributions of mean sea surface temperature in August (see *Climap Project Members* [1976] and *U.S. Navy Hydrographic Office* [1964] for Climap and modern sea surface temperature distributions, respectively). Figure 2 shows the geographical distribution of this difference in sea surface temperature as well as the margin of 18,000 yr B.P. sea ice. The distributions of topography (including ice sheets) and albedo of the continental surface as determined by the *Climap Project Members* [1976] are shown in Figures 3 and 4, respec-

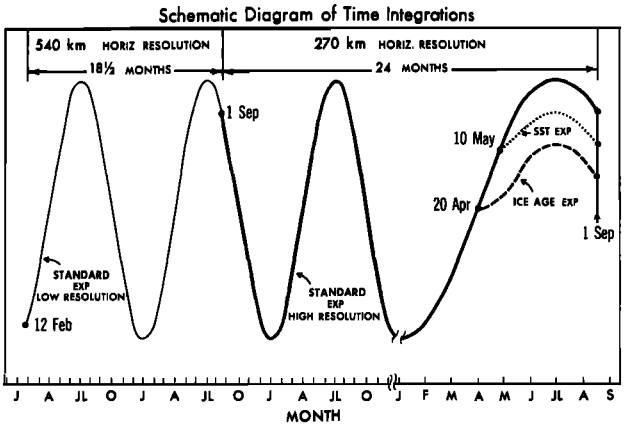

Fig. 1. Schematic diagram illustrating the time integrations of the standard, SST, and ice age experiments. The ordinate represents a climatic variable, such as temperature.

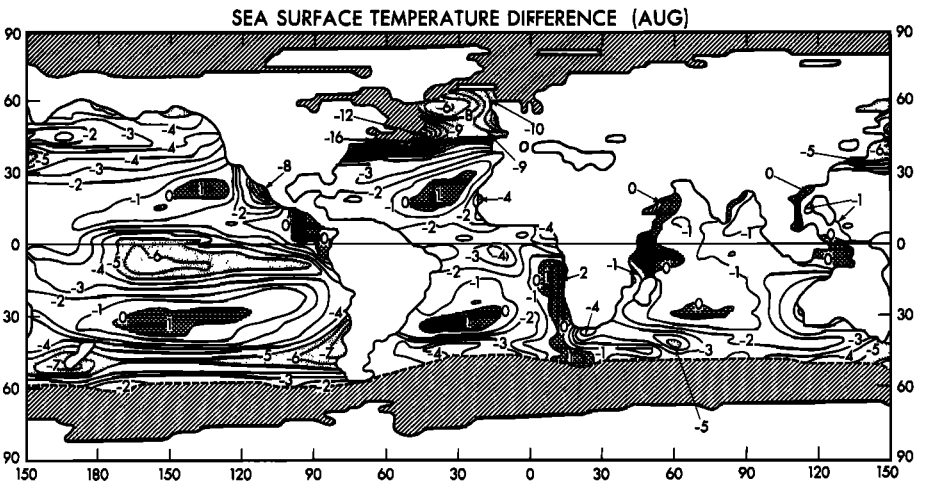

Fig. 2. Difference between Climap (18,000 yr B.P.) and present distributions of August mean sea surface temperature (in degrees Celsius). The 18,000 yr B.P. sea ice margin is indicated by shading.

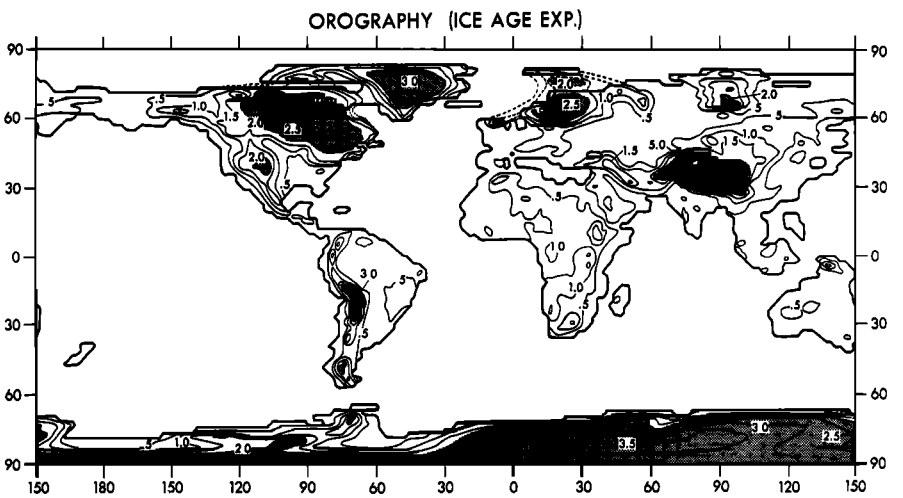

Fig. 3. Geographical distribution of surface elevation (in kilometers) of the ice age experiment as derived from the Climap reconstruction. The region of the error in topography is indicated by dashed lines.

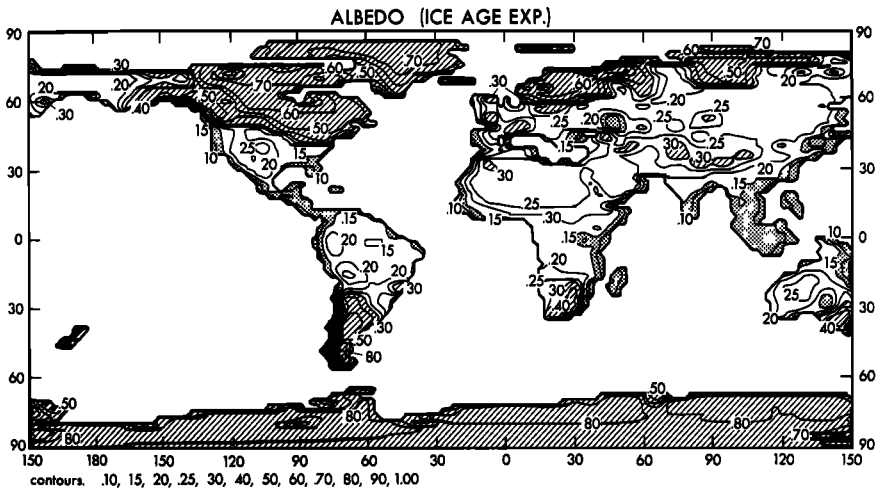

Fig. 4. Geographical distribution of land albedo of the ice age experiment as derived from the Climap reconstruction.

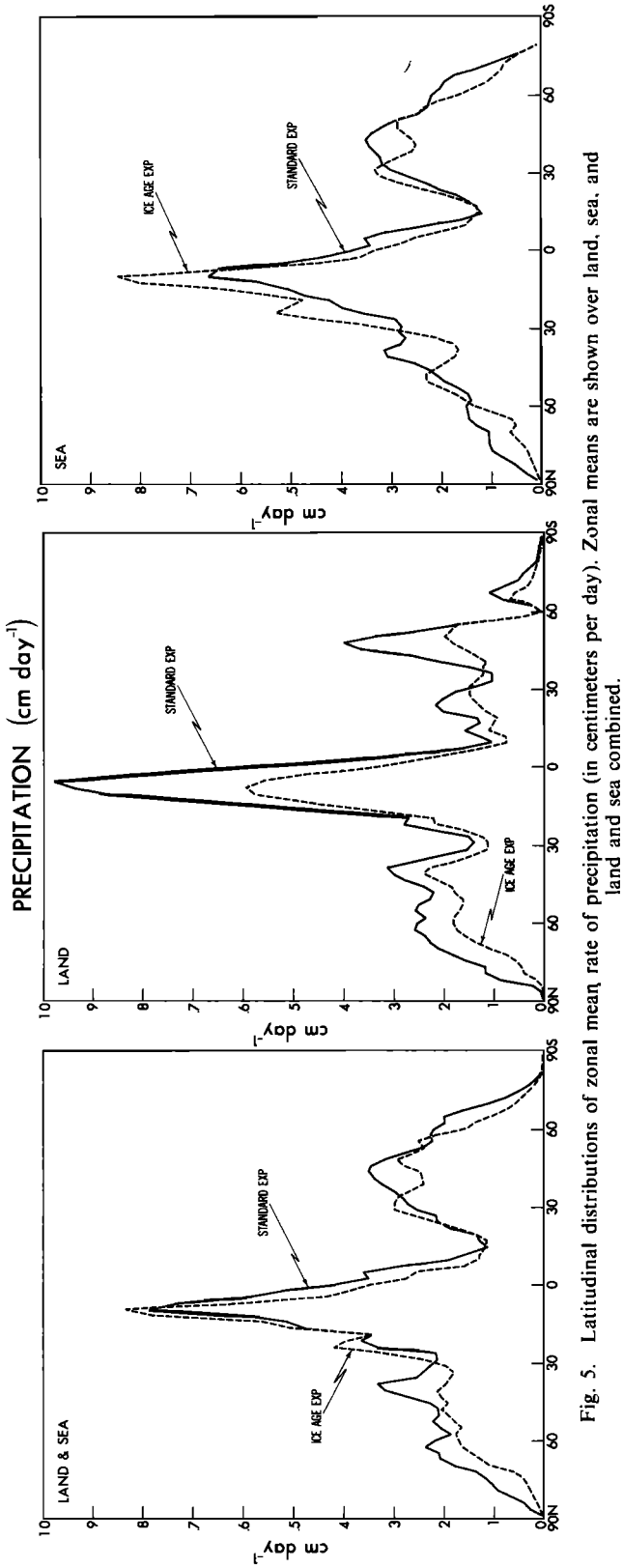

Fig. 5. Latitudinal distributions of zonal mean rate of precipitation (in centimeters per day). Zonal means are shown over land, sea, and land and sea combined.

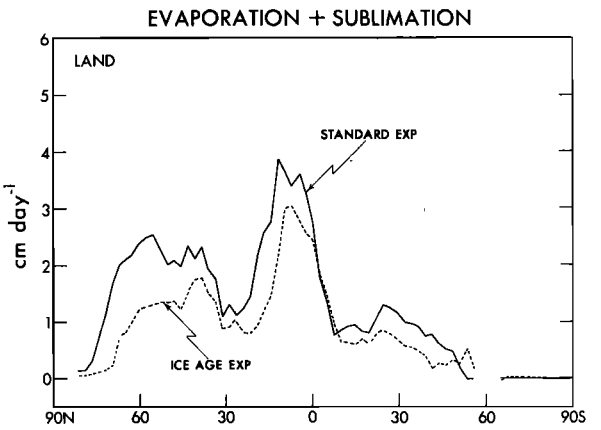

Fig. 6. Latitudinal distributions of zonal mean rate of evaporation + sublimation (in centimeters per day) over continents.

tively. The distribution of the 18,000 yr B.P. continental boundary is determined by assuming that the 18,000 yr B.P. sea level is lower than the present sea level by 80 m as suggested by Climap.

The third experiment is called the sea surface temperature (SST) experiment. It assumes the distributions of sea ice and sea surface temperature which are used for the ice age experiment but adopts the modern boundary conditions of glacial ice, surface albedo (of snow-free areas), orbital parameters, continental outlines, and topography, which are used for the standard experiment. The initial condition for this experiment is the state of the model atmosphere on May 10 in the last year of the integration of the standard experiment. As Figure 1 indicates, this integration is continued until September 1. For economy of computer time the period of the time integration is chosen to be 114 days, which is shorter than that of the ice age experiment.

It is expected that comparison of the results from the SST and standard experiments (see Table 1) may be useful for identifying the climatic response to the anomalous distribution of sea surface temperature and sea ice during the last glacial

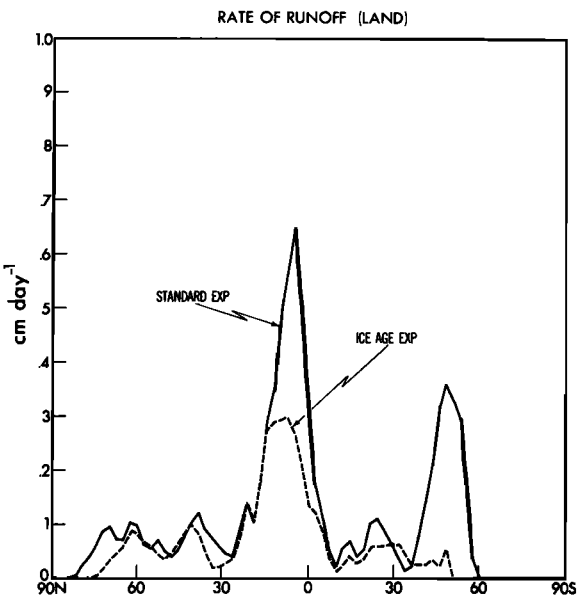

Fig. 7. Latitudinal distributions of zonal mean rate of runoff (in centimeters per day) over continents.

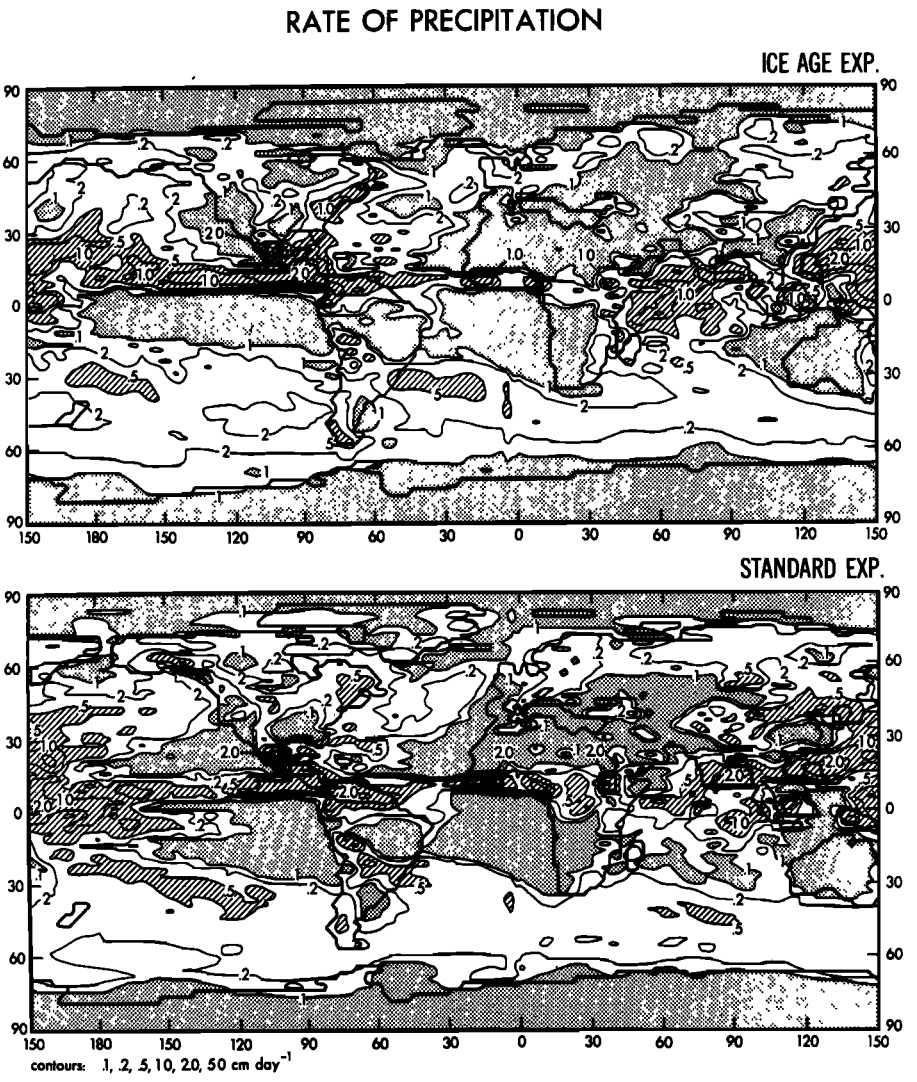

Fig. 8*a*. Geographical distributions of rate of precipitation (in centimeters per day): (top) ice age experiment and (bottom) standard experiment.

maximum. On the other hand, comparison of the results from the ice age and SST experiments can yield some insight on the response to the continental boundary conditions of the ice age, in particular, higher surface albedo and alteration of surface topography by continental ice sheets. In addition, the earth's orbital parameters are different for the ice age experiment [*Venekar,* 1972]. However, it is not probable that the small changes in orbital parameters have a significant influence upon the tropical model climate, which is the main subject of this study. This is because the changes in orbital parameters have little effect upon the seasonal variation of insolation in low latitudes. Furthermore, the distribution of sea surface temperature is prescribed in these experiments rather than internally determined. This tends to reduce the effect of orbital parameter changes on the model climate markedly.

Finally, comparisons between the ice age and standard experiments may be useful for determining the combined effects of all ice age boundary conditions. All comparisons in the following sections are, unless otherwise stated, of model results which are time-averaged over the last 2 months (July and August) of model integrations. In order to make these comparisons valid it is necessary to ascertain that the period of time integration of both the ice age experiment and the SST experiment is long enough that the initial conditions become insignificant before the beginning of the July-August analysis period. This is shown in Appendix 1.

After the completion of the ice age experiment it was found that elevations of some portions of the ice sheets were incorrectly specified because of an error in the computer program. Specifically, portions of the ice sheets which extend over oceanic areas are reduced to sea level and are replaced by sea ice with a thickness of 2 m. In Figure 3, portions of ice sheets, which are affected by this code error, are indicated by dashed lines. According to this figure the alteration of orography due to this error is limited to very high latitudes (i.e., over Hudson's Bay and the North Sea). Therefore the influence of the code error upon the tropical climate of the ice age simulation is thought to be small.

HYDROLOGIC CYCLE

Zonal means. Latitudinal distributions of the zonal mean rate of precipitation for the ice age and the standard experiments are illustrated in Figure 5. Separate illustrations are indicated for zonal means taken over land, sea, and land and sea combined. Over land and sea combined, the zonal mean rate of precipitation of the ice age simulation is smaller than

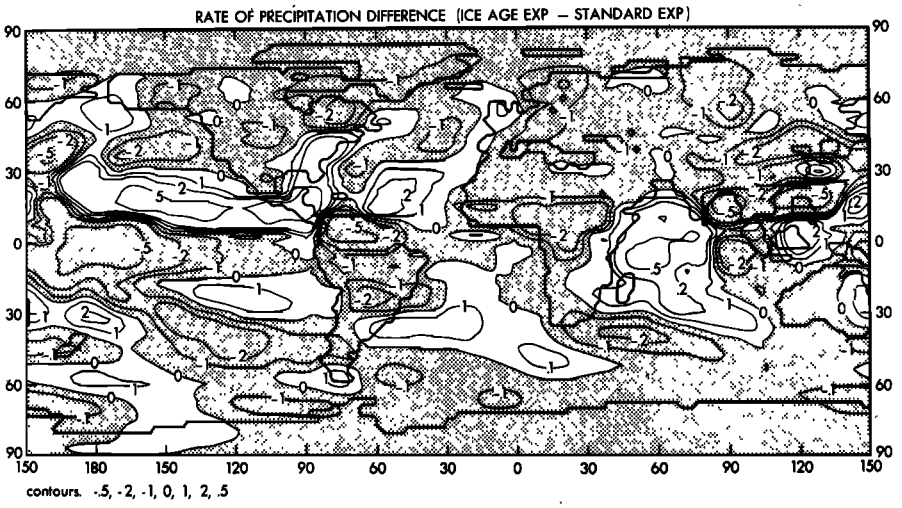

Fig. 8*b*. Geographical distribution of the difference in precipitation rate (in centimeters per day) (ice age experiment – standard experiment). Difference values have been smoothed (using a five-element filter with weights proportional to the binomial coefficients) in order to emphasize the large-scale features.

that of the standard simulation at most latitudes. However, the opposite is the case in the 10°–30°N latitude belt, which contains the tropical rain belt in the ice age simulation. This result appears to be consistent with the idea of pluvial tropics during the ice age as mentioned in the introduction. However, this increase in the zonal mean precipitation rate results from an increase over oceanic regions of the model, as will be described below.

Over tropical oceans the zonal mean rate of precipitation in the ice age simulation is significantly larger than the standard rate in the latitude belt from 5° to 30°N and slightly larger in the belt from 15° to 30°S. The ice age rate, however, is smaller in the belt from 5°N to 15°S. As will be discussed later, the difference described above tends to be closely related to the latitudinal distribution of zonal mean sea surface temperature difference (see Figure 14).

Over continents the zonal mean precipitation rate of the ice age simulation is generally smaller than that of the standard simulation. This difference is particularly large in low latitudes and contributes to the aridity of tropical continents, as will be discussed below. In order to evaluate the surface aridity it is necessary to evaluate not only the precipitation rate but also the evaporation rate, which is shown in Figure 6. This figure indicates that at nearly all latitudes the zonal mean rate of evaporation over continents in the ice age simulation is significantly less than the corresponding rate of evaporation in the standard simulation. Since the difference in evaporation rate almost balances the difference in precipitation rate, there is a relatively small difference in the amount of water available for runoff at most latitudes. However, for tropical land areas the difference in the evaporation rate is much less than the difference in the precipitation rate. Therefore the amount of water available for runoff in the ice age simulation is substantially less than the amount available in the standard experiment. This is evident in Figure 7, which shows latitudinal distributions of the zonal mean rate of runoff over continents for both simulations. In short, these results clearly demonstrate that tropical continents in the ice age simulation are more arid than those in the standard simulation, a finding in agreement with recent geological evidence [e.g., *Street and Grove*, 1976].

One of the important reasons for the reduction of evapora-

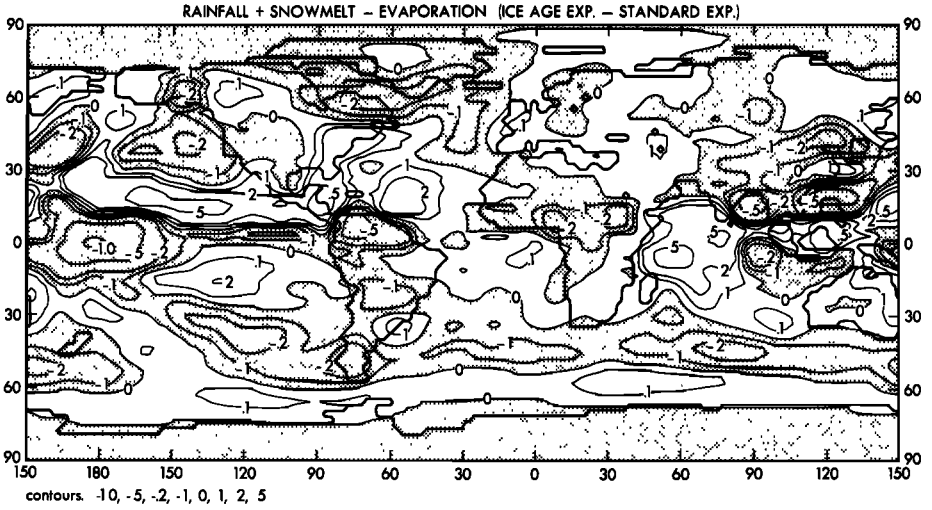

Fig. 9. Geographical distribution of the difference (ice age experiment – standard experiment) in net water supply (rainfall + snowmelt – evaporation) (in centimeters per day). Values have been smoothed as they were in Figure 8*b*.

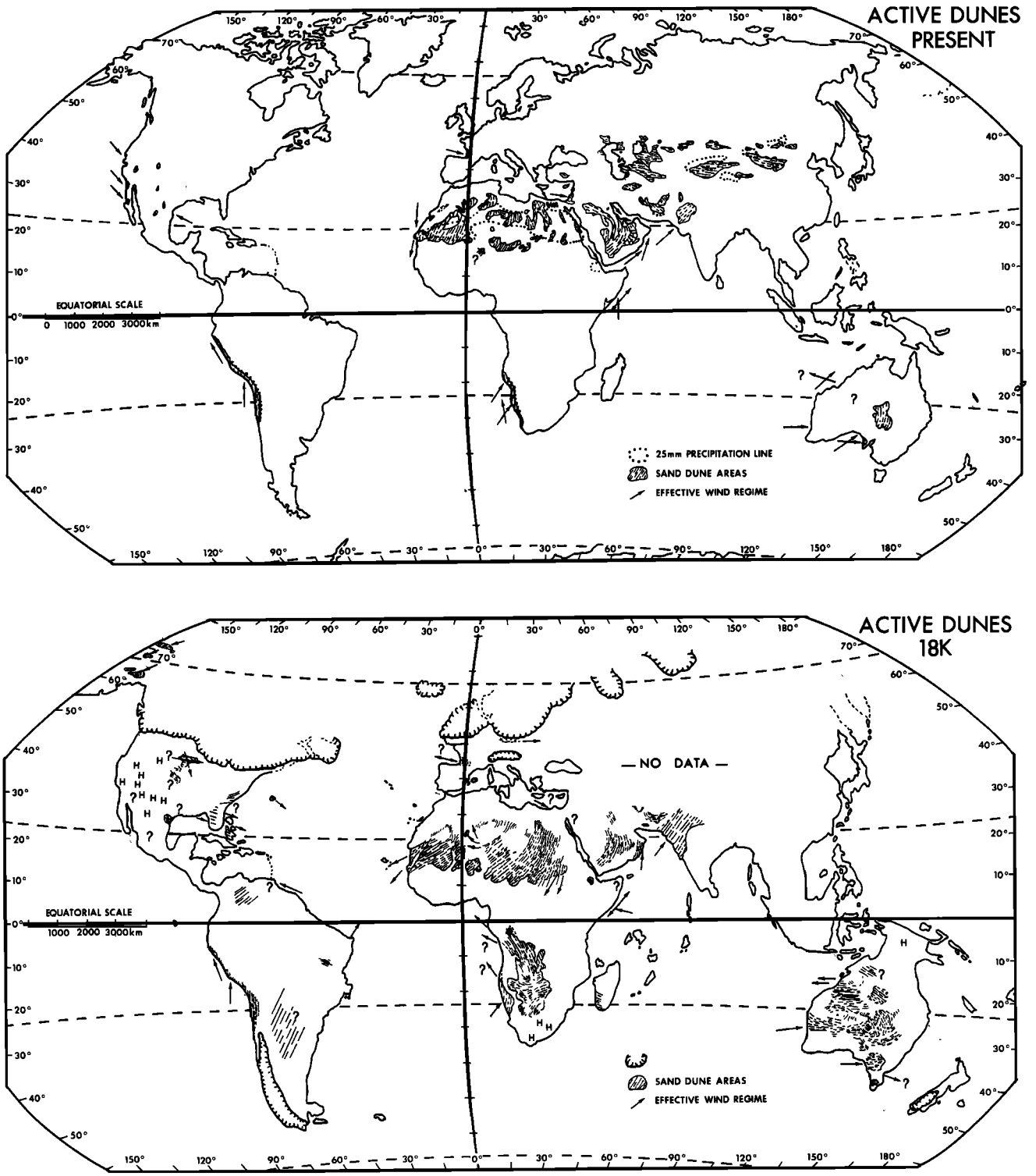

Fig. 10. Geographical distributions of active sand dunes (hand-copied from *Sarnthein and Diester-Haass* [1977]): (top) present distribution and (bottom) 18,000 yr B.P. distribution. Spiral lines indicate the margins of glacial ice.

tion rate described above is that for ice age continents, generally larger values of surface albedo are prescribed. Since larger surface albedo reduces the amount of solar energy available for evaporation, it is reasonable that the rate of evaporation of the ice age experiment is lower than that of the standard experiment. In addition, generally lower temperatures at the earth's surface in the ice age simulation are responsible for a further reduction in the evaporation rate. As is indicated by the Clapeyron-Clausius relationship, saturation vapor pressure decreases with decreasing temperature. Therefore given a net downward radiative flux at the earth's surface, which must be equal to the sum of upward surface fluxes of sensible heat and latent heat of evaporation, the portion of heat used for evaporation decreases sharply with decreasing surface temperature. Obviously, this mechanism reduces the evaporation rate over not only continental but also oceanic surfaces and ac-

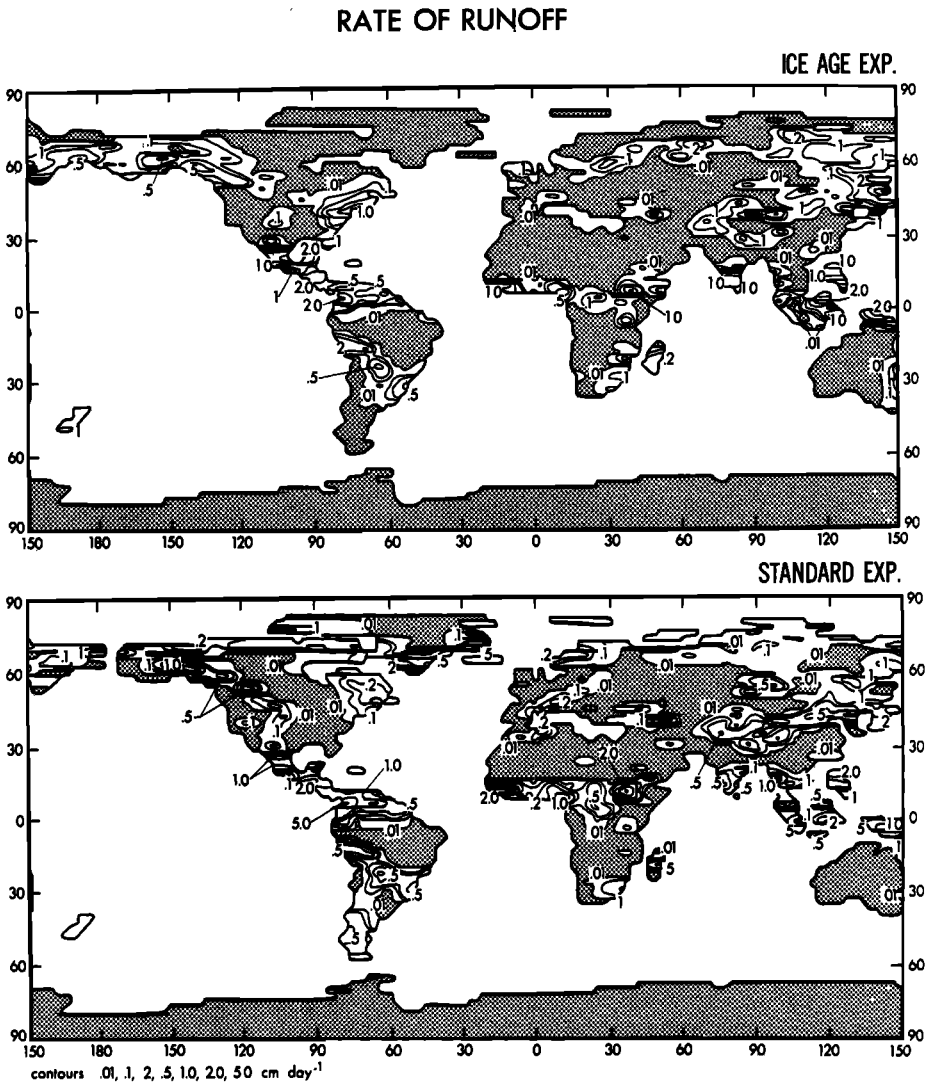

Fig. 11. Geographical distributions of the rate of runoff (in centimeters per day): (top) ice age experiment and (bottom) standard experiment.

counts for the relative weakness of the overall intensity of the hydrologic cycle in the ice age experiment. For further information regarding the overall intensity of the hydrologic cycle, refer to Table 2 of Appendix 3, a table which includes area integrals of the rate of precipitation for both the standard and ice age experiments.

Geographical distributions. Geographical distributions of the precipitation rate obtained from the ice age and standard experiments are shown in Figure 8*a*. For ease of comparison a map of the difference in precipitation rate between the two experiments is also shown in Figure 8*b*. An extensive discussion of the distribution of precipitation rate in the standard simulation was presented by *Manabe and Holloway* [1975]; therefore it is not repeated here. Instead, the present study deals mainly with differences in precipitation rates between the two experiments. According to Figure 8*b*, precipitation over the tropical continents (i.e., tropical Africa, the northernmost portion of South America, and much of southern Asia) is much less in the ice age simulation. If one compares the distribution of the difference in precipitation rate shown in Figure 8*b* with the corresponding distribution of sea surface temperature differences shown in Figure 2, one notes some correspondence between the two distributions over tropical model oceans. For example, the areas of large negative sea surface temperature difference along the equator in the eastern Pacific correspond to areas of large rainfall reduction. In addition, areas of small positive sea surface temperature difference in the Atlantic and the eastern Pacific just north of the equator coincide well with areas of rainfall increase. In general, the correspondence between the two differences is much better in the tropics of the northern hemisphere than in that of the southern hemisphere.

In Appendix 2 the statistical significance of the difference in precipitation rate between the two simulations is evaluated on the basis of the signal-to-noise ratio computation proposed by *Leith* [1973]. This evaluation indicates that the following features of the difference field are significant: (1) the large reduction in precipitation rate over tropical Africa and Venezuela and (2) the changes in precipitation rate over the tropical oceans in the northern hemisphere as identified in the preceding paragraph.

Some of the features of the precipitation difference field, as described above, are not evident in the results of *Gates* [1976*b*]. In particular, Figure 23 of Gates indicates that the rate of precipitation over equatorial Africa and northern portions of South America of the ice age simulation is significantly larger

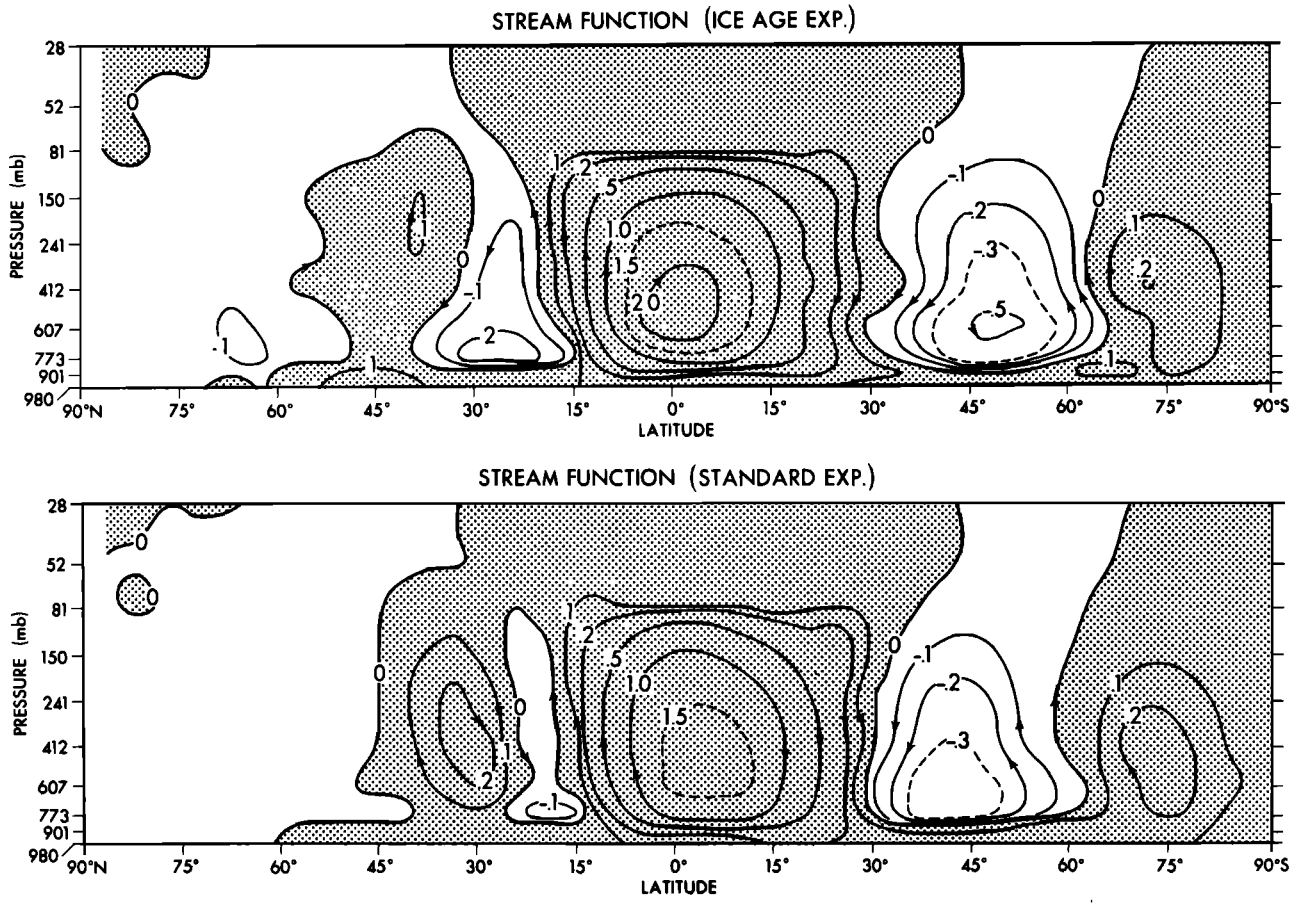

Fig. 12. Stream function of mean meridional circulation (10^{13} g s^{-1}): (top) ice age experiment and (bottom) standard experiment. Zonal means are taken over both continents and oceans.

than that of the standard simulation, features which are at variance with results from this study. Gates pointed out that his standard simulation of the geographical distribution of the rate of precipitation is in relatively poor agreement with observations. Therefore it is our contention that the present results are more reliable than Gates's results with regard to the distribution of precipitation in the tropics.

As has been pointed out already, reduction in precipitation rate does not necessarily imply a change in the aridity of the continental surface. Therefore the geographical distribution of 'net water supply' is computed. This quantity indicates the difference between the water gain at the surface (rainfall and snowmelt) and the water loss (evaporation). Positive values indicate increased availability of water for runoff (or for increasing soil moisture) for continental regions and reduction of salinity for oceanic regions. Figure 9 illustrates the distribution of the difference in net water supply between the ice age and standard experiments. This figure reveals that over equatorial Africa, the northern part of South America, and southern Asia (i.e., over the Himalayas and the northern portions of India and Burma), surface conditions are much drier in the ice age simulation than in the standard simulation. In other words, the results of these numerical experiments suggest that most of the tropical continental areas were drier during the last ice age.

Although it may not be reasonable to infer too much from the ice age experiment, in which only one season (July-August) is simulated, it is nevertheless of interest to examine these results in light of the geological record. Figure 10 illustrates geographical distributions of sand dunes, which were compiled by *Sarnthein and Diester-Haass* [1977]. This figure, which contains modern and 18,000 yr B.P. distributions of sand dunes, indicates that during the ice age, sand dunes developed extensively in the northern portions of tropical Africa, where savannah grows at present, and in Angola and its neighborhood, the Orinoco river basin of Venezuela, and the northwestern part of India. These areas approximately coincide with areas where the net water supply of the ice age experiment is significantly smaller than that of the standard experiment.

It is known that during August, tropical rain belts over continents shift to their northernmost latitudes. A manifestation of this characteristic of the earth's climate is that the Sahel region of Africa, the Orinoco region of South America, and the general region of south Asia receive nearly all of their rainfall in the season (July-August) which corresponds with the analysis period of these simulation studies. Accordingly, it is quite probable that these regions would remain relatively dry even if the time integration of the ice age experiment were extended from one season to an entire year. In view of this consideration the aridity of the aforementioned regions in the ice age simulation is generally more significant.

As one may expect, the difference in net water supply between the two experiments affects the difference in the rate of runoff. Figure 11 shows geographical distributions of the rate of runoff which are obtained from both the ice age and standard experiments. Again, this figure clearly shows that in tropical Africa and Venezuela the rate of runoff of the ice age experiment is significantly less than that of the standard ex-

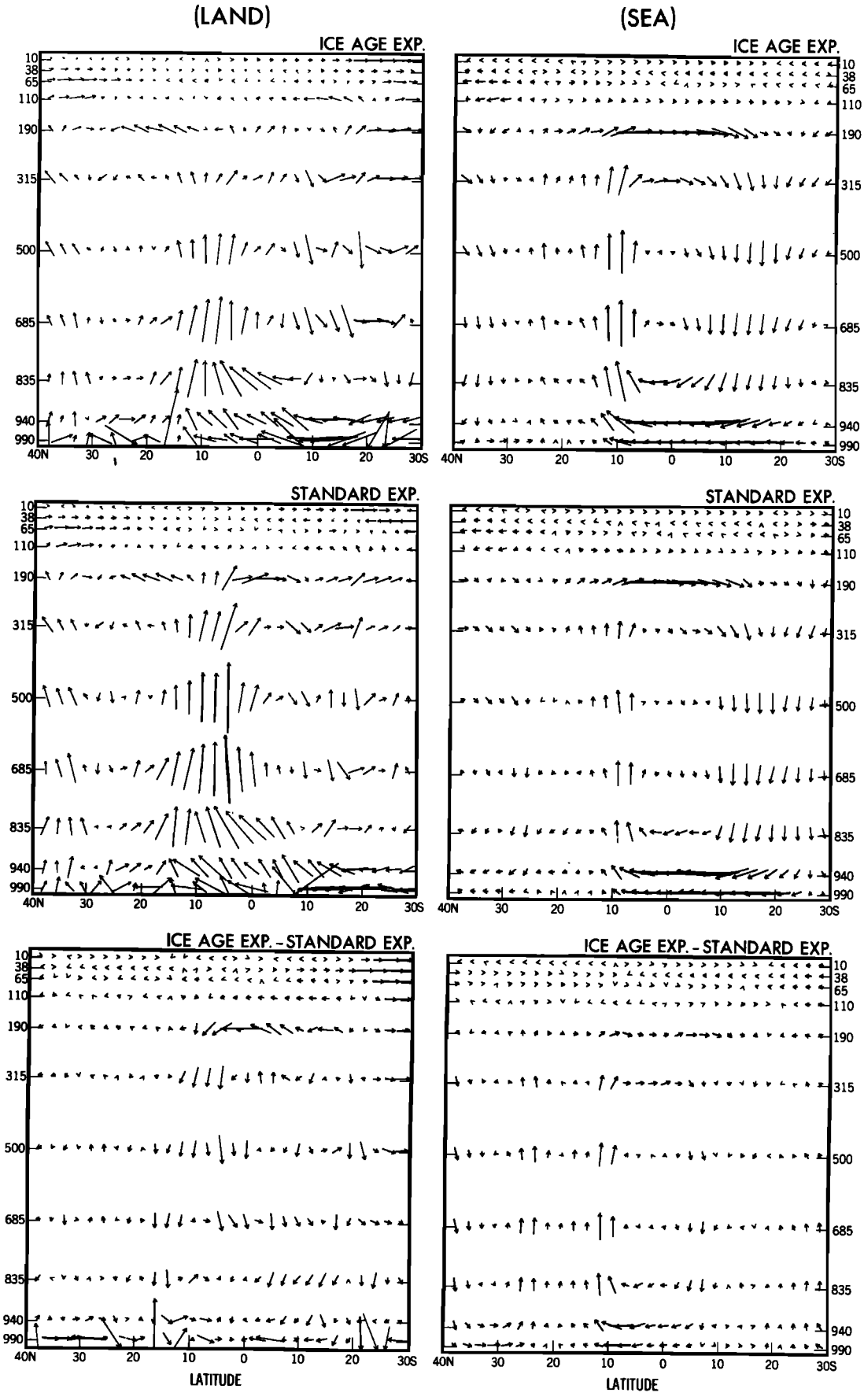

Fig. 13. Zonal mean meridional circulation over land and sea: (top) ice age experiment, (middle) standard experiment, and (bottom) ice age experiment − standard experiment. The length of a vector represents the displacement of an air parcel in 2 days.

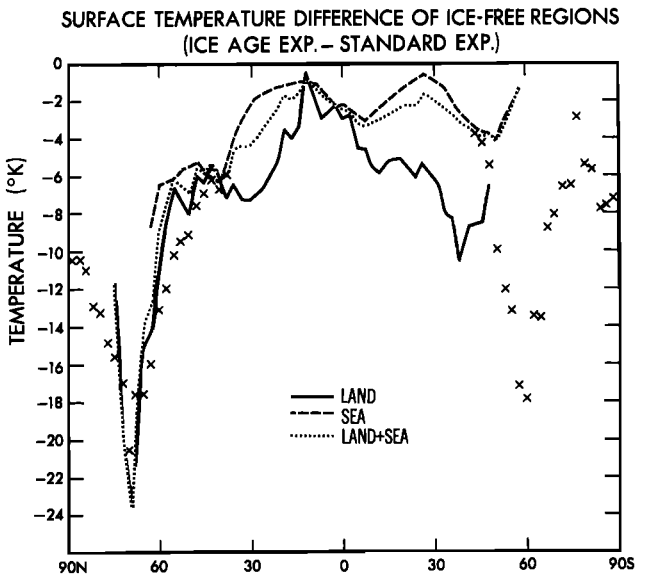

Fig. 14. Latitudinal distribution of difference (ice age experiment standard experiment) in zonal mean surface temperature (in degrees Celsius) over ice-free regions. Differences in zonal mean temperature including ice-covered regions (over land and sea combined) are shown by crosses.

periment. There is much geological evidence which indicates a reduction of runoff over the tropical continents during the last ice age. For example, it has been suggested that Lake Victoria and Lake Albert in Uganda were low for an unknown time just before 12,500 yr B.P. [*Kendall,* 1969; *Livingston,* 1971]. *Servant* [1973] concluded that Lake Chad, fed by the Logone and Ubangui-Shari river system was very low between 20,000 and 13,000 yr B.P. and high from 12,000 to 5000 yr B.P. *Darmuth and Fairbridge* [1970] pointed out that during the very late Pleistocene, deep-sea cores from the continental shelf east of Brazil show rapid deposition of abundant unweathered feldspar and coarse subangular quartz sand, suggesting limited chemical weathering. For extensive compilation of evidence supporting the reduction of runoff rate over continental tropical regions during the last ice age, see *Williams* [1975] and *Street and Grove* [1976].

There are several areas where the rate of runoff did not change significantly even though the net water supply in the ice age simulation (Figure 9) is less than that in the standard simulation, i.e., western Australia, the neighborhood of Angola, and northern India. In these regions, changes in net water supply are essentially compensated by changes in soil moisture rather than runoff. Therefore one cannot evaluate the aridity (or wetness) of these regions unless the time integration of the ice age model is extended from one season to one or more years. Also, it should be noted that over northern India the rates of precipitation and runoff in the standard simulation are much smaller than those observed [*Hahn and Manabe,* 1975], an indication that the model needs further improvement before a satisfactory evaluation of the hydrologic response of this region can be made.

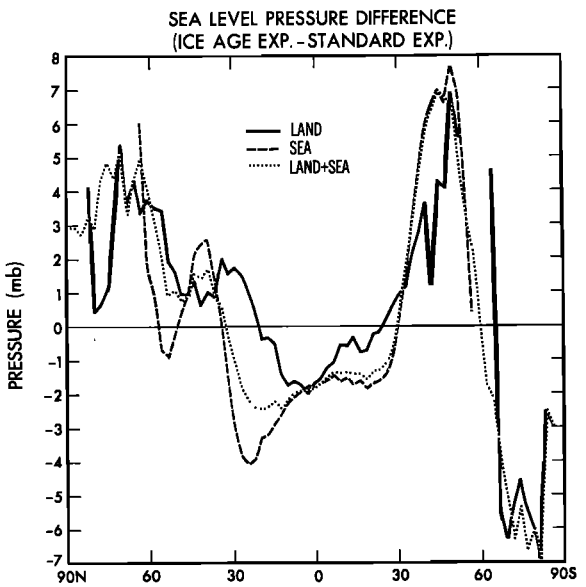

Fig. 15. Latitudinal distribution of difference (ice age experiment – standard experiment) in zonal mean sea level pressure (in millibars).

ATMOSPHERIC CIRCULATION

Zonal means. In the preceding section, differences in the rate of precipitation between the ice age and standard experiments were described. In this section, differences in the atmospheric circulation between the two simulations are described so that one can gain understanding of the mechanisms responsible for the aridity of tropical continental regions during the last glacial maximum.

Figure 12 illustrates the meridional stream function averaged over both oceanic and continental regions. According to this figure the southern Hadley cell, which straddles the equator, intensifies in response to ice age boundary conditions. The northern Hadley cell also intensifies, but in comparison to the southern Hadley cell it is very weak in both simulations. From discussions in the following paragraphs it becomes evident that the intensification mentioned above results essentially from the acceleration of meridional circulation over oceanic regions. Results from other numerical experiments are not in

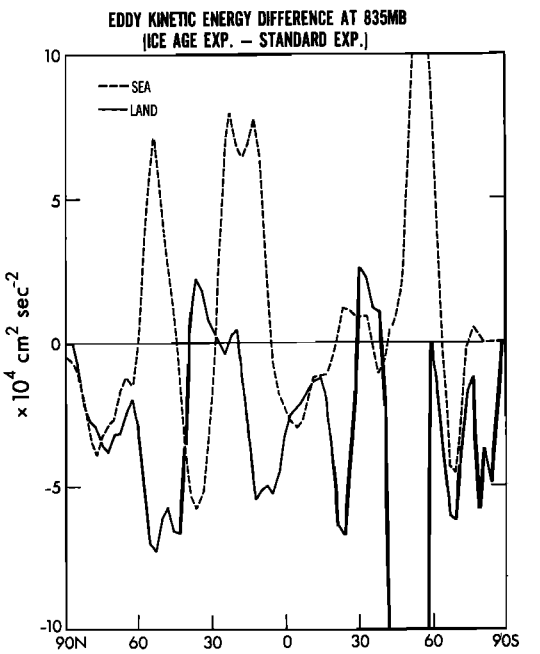

Fig. 16. Latitudinal distribution of zonal mean difference (ice age experiment – standard experiment) in kinetic energy of transient eddies (10^4 cm^2/s^2) at the 835-mbar level as defined for Figure 6.4 of *Manabe et al.* [1974].

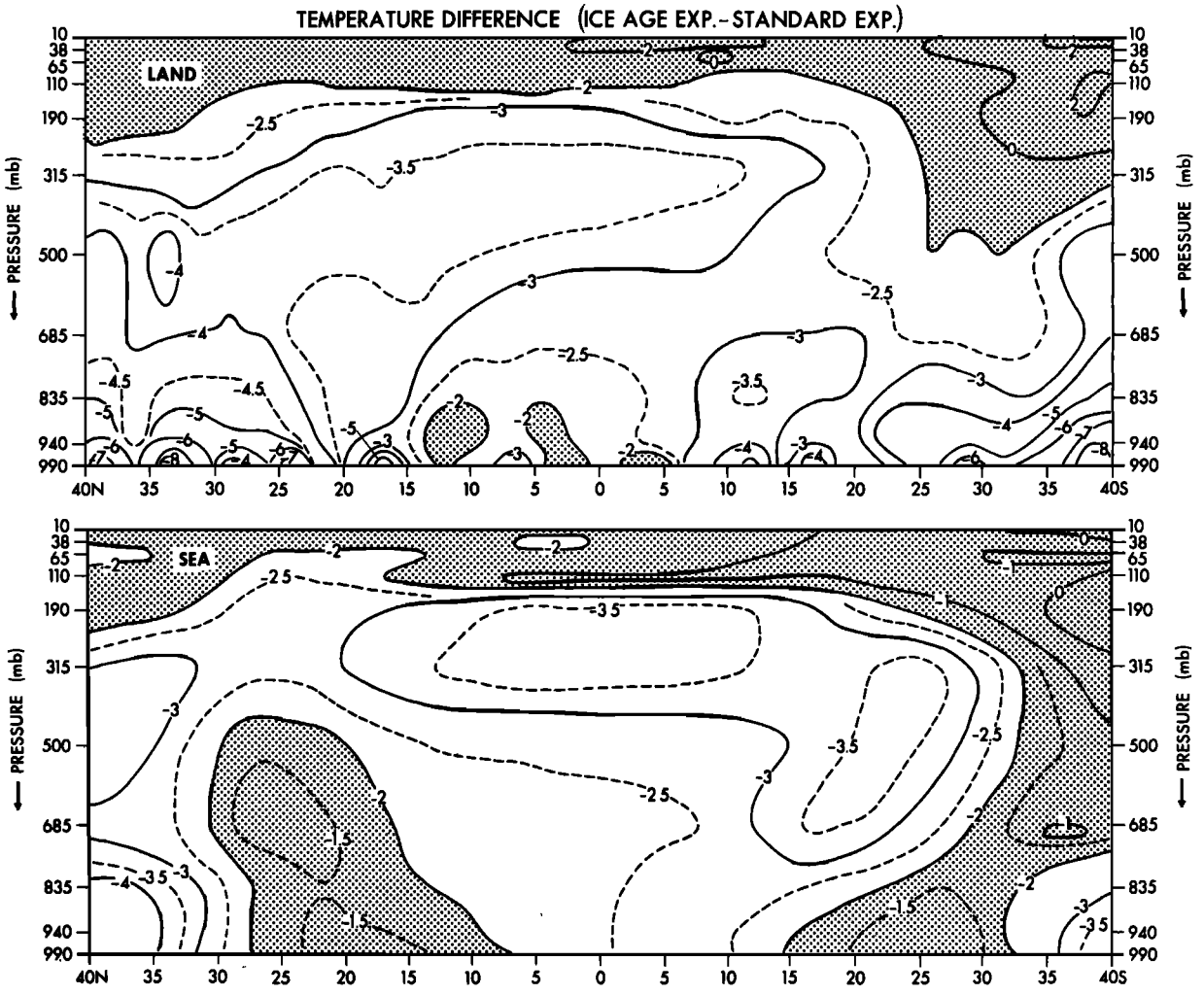

Fig. 17. Latitude-pressure distributions of zonal mean temperature difference (ice age experiment − standard experiment) (in degrees Celsius): (top) land and (bottom) sea.

agreement with one another on the intensification of the Hadley cell. For example, *Alyea* [1972] and *Saltzman and Venekar* [1975] report a more intense ice age Hadley cell, whereas *Williams* [1974] and *Gates* [1976*b*] note a weaker one. Causes for this disagreement have not been identified.

Over continental portions of the model tropics the intensity of meridional circulation weakens in response to ice age boundary conditions, as is shown by Figure 13, which illustrates the zonal mean vectors of meridional circulation over continents as a function of latitude and pressure for both

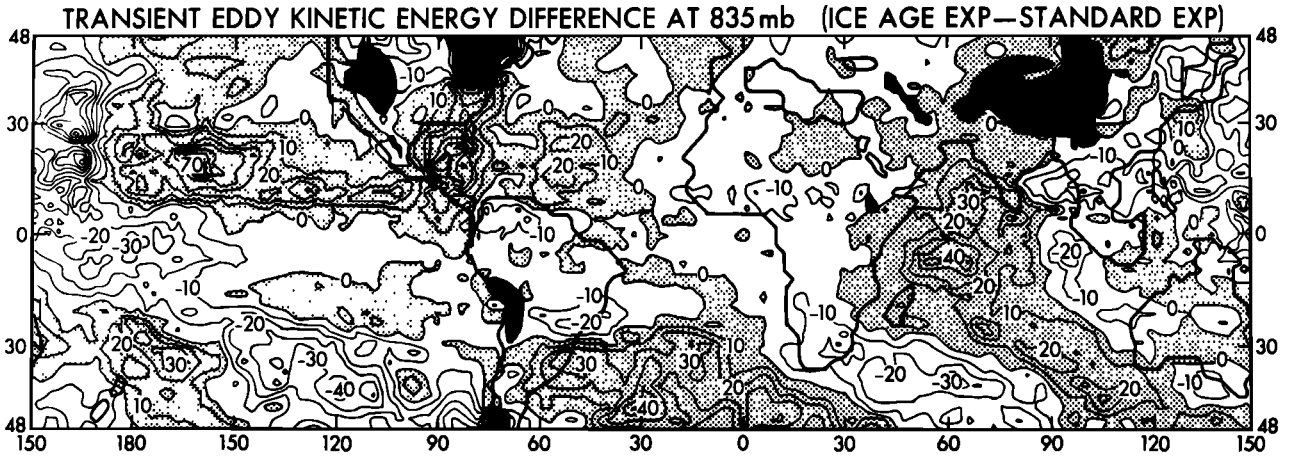

Fig. 18. Geographical distribution of difference (ice age experiment − standard experiment) in kinetic energy of transient eddies (10^4 cm^2/s^2) at the 835-mbar level as defined for Figure 6.4 of *Manabe et al.* [1974].

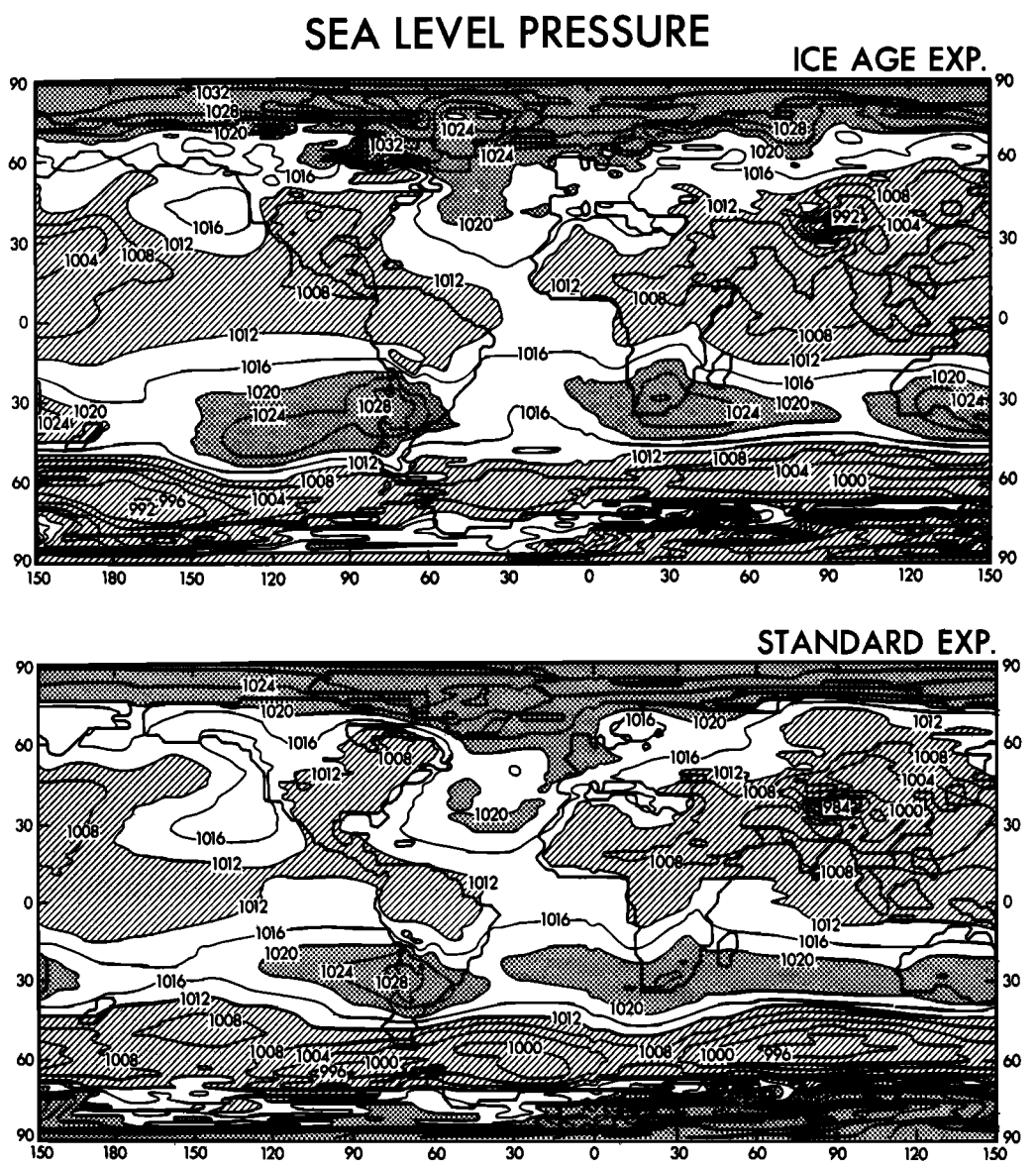

Fig. 19*a*. Geographical distribution of sea level pressure (in millibars): (top) ice age experiment and (bottom) standard experiment.

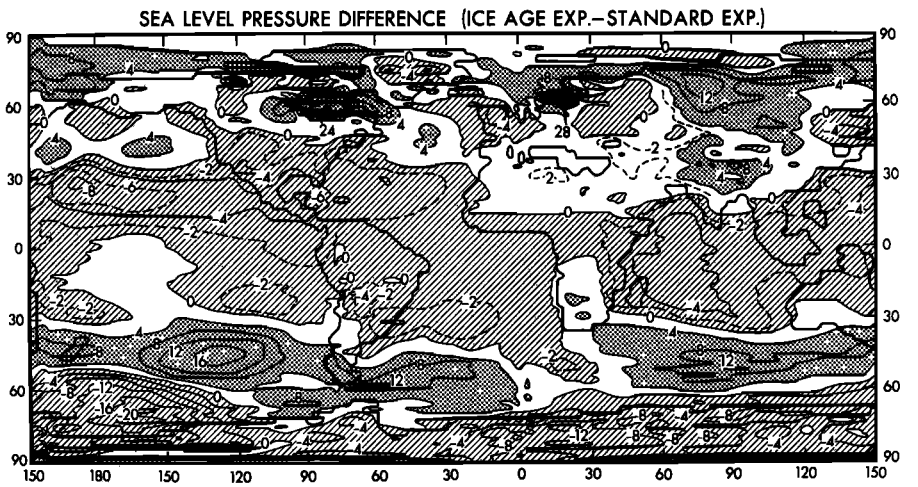

Fig. 19*b*. Geographical distribution of sea level pressure difference (in millibars) (ice age experiment − standard experiment).

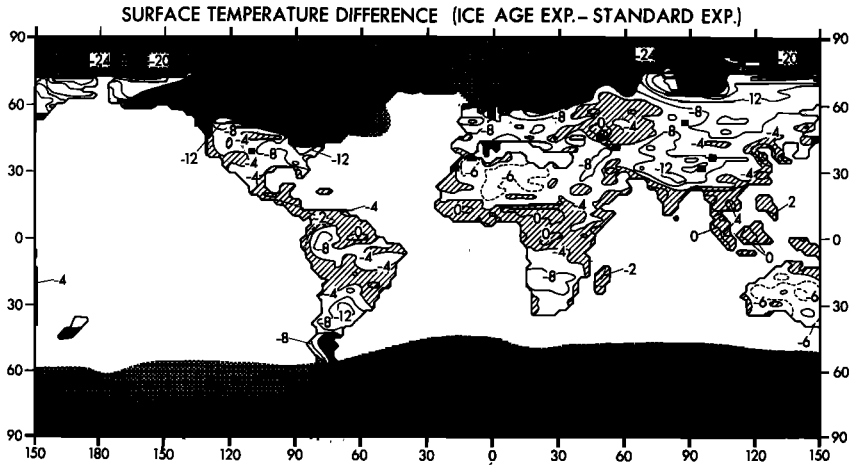

Fig. 20. Geographical distribution of surface temperature difference (in degrees Celsius) (ice age experiment − standard experiment).

simulations. In addition, the difference between the two vector fields is also included at the bottom of this figure for ease of comparison. These illustrations reveal that the flow in the upward branch of the Hadley circulation in the ice age simulation is narrower and weaker than that in the standard simulation. This is consistent with the lower rainfall rate in the tropical portion of continents in the ice age simulation as described in the preceding section.

Figure 13 also contains the corresponding oceanic distributions of meridional circulation. This figure indicates that the upward branch of the Hadley circulation (5°–30°N) over oceans is more intense in the ice age simulation than in the standard simulation. In this latitude belt the precipitation rate over oceans was previously shown to increase substantially in response to the effects of ice age boundary conditions. In addition, the downward flow branch of the Hadley cell over oceans in the ice age simulation is significantly stronger in the latitude belt ranging from 5°N to 15°S, but it is slightly weaker in the latitude belt ranging from 15° to 30°S. As was described in the preceding section, the oceanic precipitation rate in the ice age simulation is smaller from 5°N to 15°S but slightly larger from 15° to 30°S. In short, the differences in the intensities of the meridional circulation over oceans are qualitatively consistent with the differences in the precipitation rates.

Figures 14 and 15 show latitudinal distributions of zonal mean differences of surface temperature and sea level pressure averaged over land and sea combined. In tropical regions of the ice age experiment, surface temperature differences tend to be small in comparison with the large temperature differences found at higher latitudes. In response to the surface temperature distribution described here, sea level pressure tends to be generally lower in low latitudes and higher in middle latitudes in the ice age experiment. The reduction in the subtropics is more pronounced in the northern hemisphere than in the southern hemisphere. This difference contributes to intensifying the thermally direct southern Hadley cell.

For the tropics a more detailed understanding of the differences in the circulation, described above, is gained by looking at zonal mean differences taken separately over land and sea. Figures 14, 15, and 16 show such differences for surface temperature, sea level pressure, and kinetic energy of transient eddies at the 835-mbar level, respectively. These figures indicate that over oceanic portions of the 5°–30°N latitude belt,

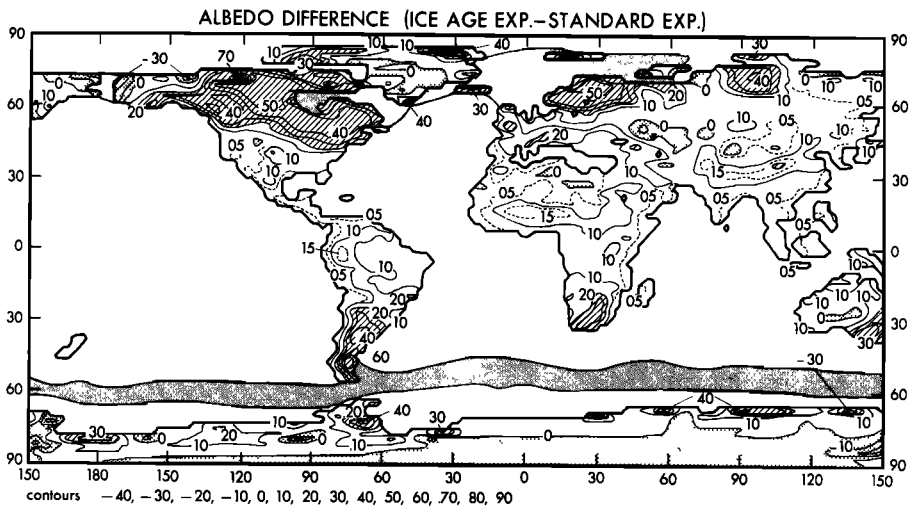

Fig. 21. Geographical distribution of surface albedo difference (ice age experiment − standard experiment). The light shading over the oceans indicates the change in the sea-ice margin.

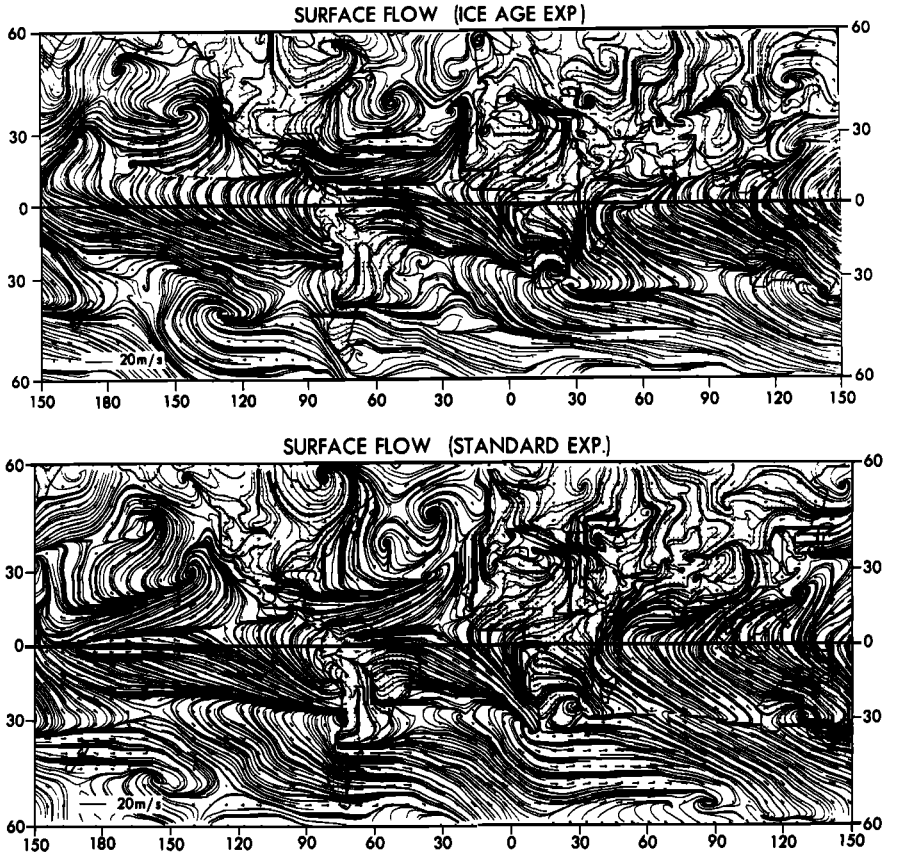

Fig 22*a*. Geographical distributions of surface wind vectors: (top) ice age experiment and (bottom) standard experiment.

surface temperature difference is at a minimum where the reduction of sea level pressure is at a maximum and the precipitation rate and eddy kinetic energy increase. On the other hand, the sea surface temperature difference is at a maximum in the latitude belt around 7°S, where sea level pressure reduction is at a local minimum and the precipitation rate and eddy kinetic energy decrease. In other words, precipitation rate, moist convective activity, and the intensity of tropical cyclones increase in response to ice age boundary conditions in the belt of minimum sea surface temperature difference (i.e., the 5°–30°N belt), whereas they decrease in the belt of maximum sea surface temperature difference. Here, it is important to note that the increase in precipitation rate mentioned above occurs despite the possible reduction in the

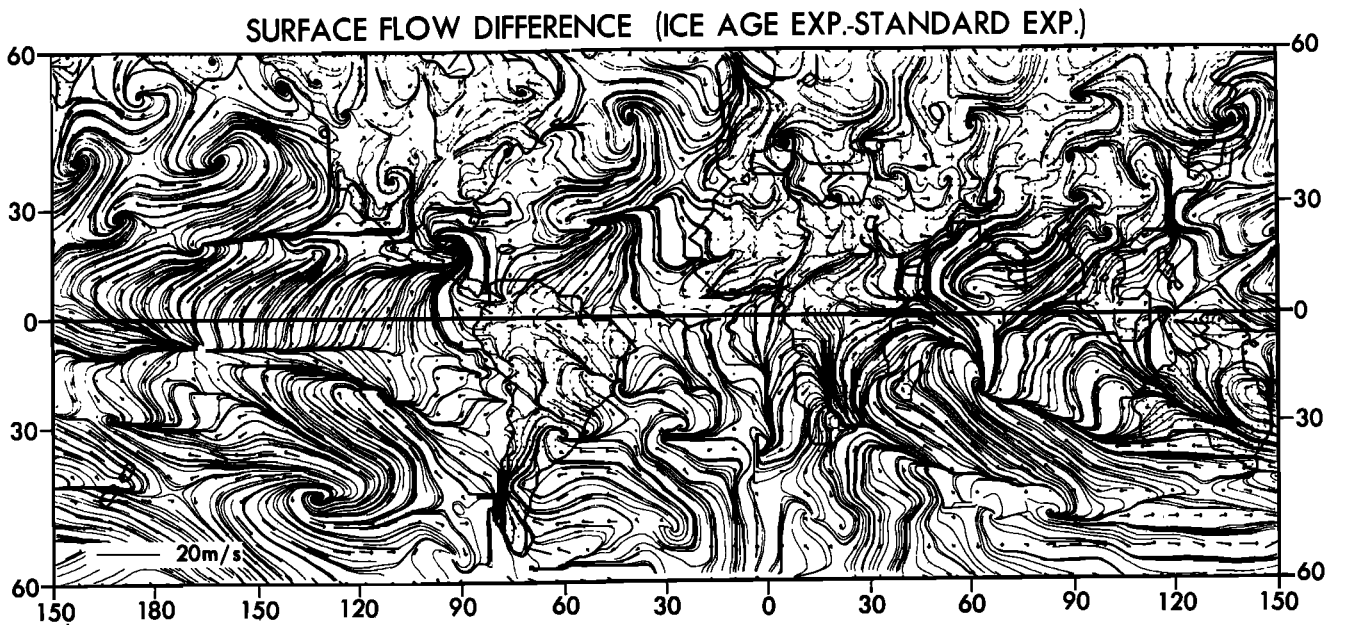

Fig. 22*b*. Geographical distribution of surface wind vector difference (ice age experiment − standard experiment).

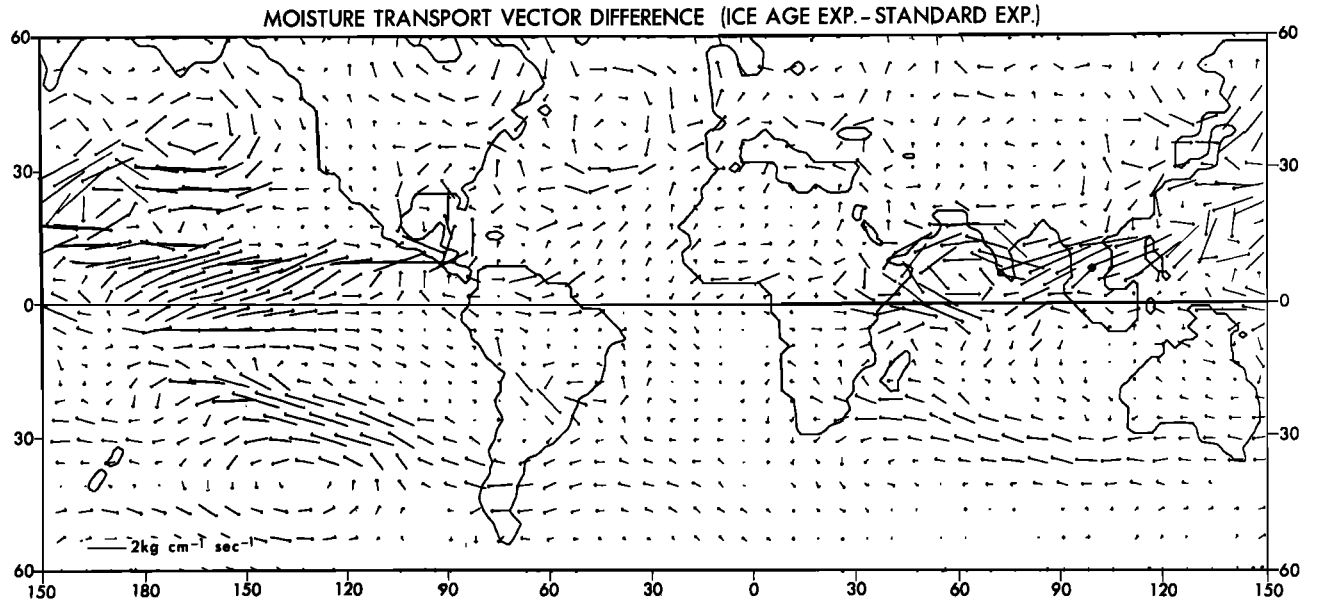

Fig. 23. Geographical distribution of the vector difference in moisture transport by the stationary component of the flow (ice age experiment − standard experiment).

evaporation rate due to the slight lowering of sea surface temperature in the belt of minimum difference.

In earlier papers, *Manabe et al.* [1970, 1974] analyzed the behavior of the global model used for this study and concluded that both the intensity of moist convection and the activity of tropical cyclones are at a maximum in the neighborhood of maximum sea surface temperatures. They showed that in such a region the rate of latent heat release is at a maximum and a warm core develops in the upper (or middle) troposphere, creating a circumstance which is favorable for the release of potential energy and the development of tropical cyclones. In the belt of minimum sea surface temperature difference (5°–30°N) in the ice age experiment, sea surface temperatures tend to be warmer in comparison to neighboring areas, an increased temperature contrast with surroundings thus being maintained. Therefore it is reasonable that the level of activity of tropical cyclones and the precipitation rate in the ice age experiment are significantly higher in this belt than those of the standard simulation but are significantly lower in the belt of maximum sea surface temperature difference located just south of the equator.

It is important to recognize that in the belt of minimum sea surface temperature difference located around 20°S the differences in sea level pressure, eddy kinetic energy, and precipitation rate between the two simulations are much less than those in the similar belt located north of the equator. The reason for this may become evident if one recalls that the 25°S belt is situated in the dry downward-moving branch of the southern (main) Hadley cell. Furthermore, sea surface temperature and evaporation rates in this belt are much lower than those in the northern belt. In short, the 25°S belt is much less favorable for moist convective activity than the northern belt, and accordingly, the sea level pressure difference between the two simulations around 25°S is much less pronounced than the local maximum around 25°N. Therefore the cross-equatorial surface pressure gradient in the ice age simulation is significantly larger than that in the standard simulation. This difference in meridional pressure gradient around the equator accounts for the difference in the intensity of the southern (main) Hadley cell which was described earlier.

In tropical latitudes of the ice age experiment, continental surface temperatures are, in general, reduced more than oceanic surface temperatures. From hydrostatic considerations it is therefore reasonable that the land-to-sea sea level pressure gradient is increased in the tropics of the ice age experiment, as Figure 15 indicates. This differential response in sea level pressure between land and sea areas produces increased outflow of near-surface air from continental to oceanic regions, which in turn contributes to the maintenance of more arid conditions in tropical continental regions of the ice age experiment.

It is interesting to note, however, that the continental difference in surface temperature at 2°–13°N is almost as small as the oceanic difference near 20°N. Nevertheless, the continental sea level pressure difference in the 2°–13°N belt is weaker than

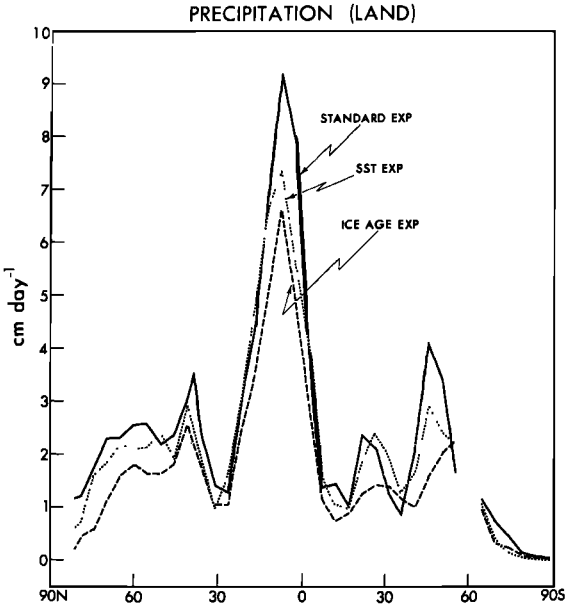

Fig. 24. Latitudinal distributions of zonal mean rate of precipitation (in centimeters per day) over land.

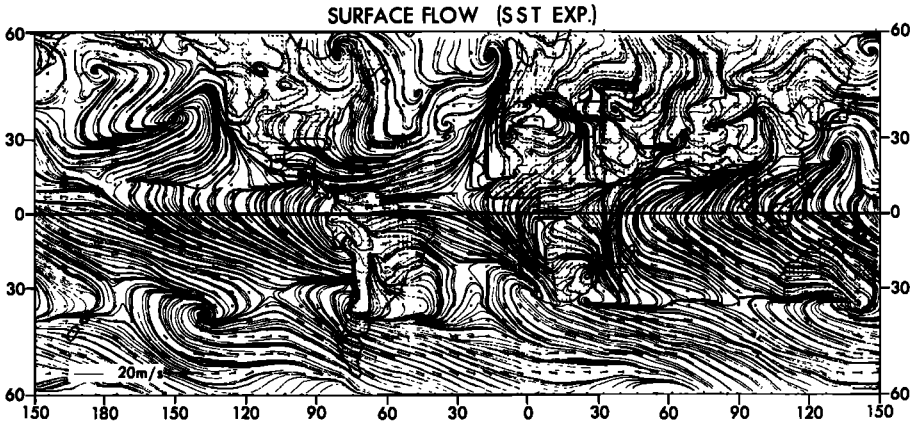

Fig. 25. Geographical distribution of surface wind vectors and streamlines of the SST experiment.

the oceanic low-pressure difference near 20°N. In order to appreciate this result it is necessary to examine the temperature difference not only of the earth's surface but also of the upper air. Figure 17 illustrates the latitude-pressure distribution of the zonal mean temperature difference between the ice age and standard simulations; these zonal means are taken over continents and oceans separately. According to this figure the oceanic region of small temperature difference located around 20°N extends much higher in the troposphere than the continental counterpart located around 2°–13°N. This explains why the oceanic maximum of sea level pressure difference located around 20°N is much more pronounced than the continental maximum located in the 2°–13°N belt. As was discussed earlier, warm surface temperature anomalies over tropical oceans tend to enhance moist convection and maintain a warm core in the middle and upper model troposphere. However, warm continental surface temperature anomalies are not as effective as some oceanic counterparts in enhancing moist convection (and producing warm anomalies) because of the lack of surface heat capacity and a sufficient supply of moisture. These characteristics of the model behavior appear to be consistent with the distribution of the region of small temperature difference described above.

Geographical distribution. Over tropical oceanic regions, relationships among the mean differences in surface temperature, rate of precipitation, eddy kinetic energy, and sea level pressure are evident not only in the zonal mean distributions (as was previously discussed) but also in the geographical distributions. As has been indicated already, geographical distributions of sea surface temperature and rate of precipitation differences between the ice age and standard simulations are shown in Figures 2 and 8*b*, respectively. In addition, the distribution of the difference in kinetic energy of transient eddies at the 835-mbar level is shown in Figure 18, and the distribution of the sea level pressure difference is illustrated in Figure 19*b*. For reference, sea level pressure distributions of the ice age and standard experiments are shown separately in Figure 19*a*. Comparisons among these figures reveal that the regions of 'warm anomalies' of the eastern tropical Pacific and the tropical Atlantic coincide approximately with the regions of increased eddy kinetic energy, intensified precipitation, and reduced sea level pressure in the ice age simulation. Here, the term warm anomaly identifies the general neighborhood of the region where the sea surface temperatures during the ice age are above present values, as is indicated by cross-hatching in Figure 2. As one may expect, the regions of warm anomalies in the tropics of the northern hemisphere tend to line up around 20°N, where a zonal belt of minimum sea surface temperature difference is located. Particularly good positive correlation is evident between the difference in precipitation rate and the difference in transient eddy kinetic energy at the 835-mbar level. In addition, the enhancement of moist convective precipitation, the increase of eddy kinetic energy, and the reduction of sea level pressure take place over warm anomalies in the subtropics of the southern hemisphere of the model (e.g., in the vicinity of zonally elongated warm anomalies located at both sides of South America). As has been discussed already, however, the effects of these anomalies are not as pronounced (or as evident) as those of the anomalies in the northern hemisphere tropics because of the reasons discussed earlier.

Although zonal mean surface temperature differences over continents tend to be larger than those over oceans (Figure 14), there are some continental regions where the difference in surface temperature between the two simulations is small. For example, small surface temperature differences are found over tropical Africa and the northern part of the South American continent, where the ice age climate is much drier than the present climate (see Figures 9 and 20). Because of the dryness of the soil surface the evaporation rate is reduced, which in turn contributes to the maintenance of relatively high surface temperatures and accounts for the small surface temperature difference between the two simulations. Owing to the reduced evaporation rate and small surface heat capacity, warm anomalies (or regions of small surface temperature difference) over continents are not as effective in enhancing moist convection and reducing sea level pressure as some of their oceanic counterparts. Accordingly, a pressure gradient tends to develop between continents and oceans which is responsible for a surface outflow from (and sinking air over) continents.

One can identify another important factor which enhances the pressure gradient from continents to oceans in the ice age simulation. According to Figure 21, albedo of the continental surface in the ice age experiment tends to be substantially larger than that used for the standard experiment. This is because of (1) the difference in the extent of ice sheets with large albedo and (2) the difference in the albedo of the ice-free surface. The albedo of the ice-free surface in the ice age experiment is somewhat larger than that used for the standard experiment, partly because of differences in vegetation and coverage by snow. Since higher surface albedo values tend to lower the temperature of the surface and that of the overlying air, albedo differences contribute to higher sea level

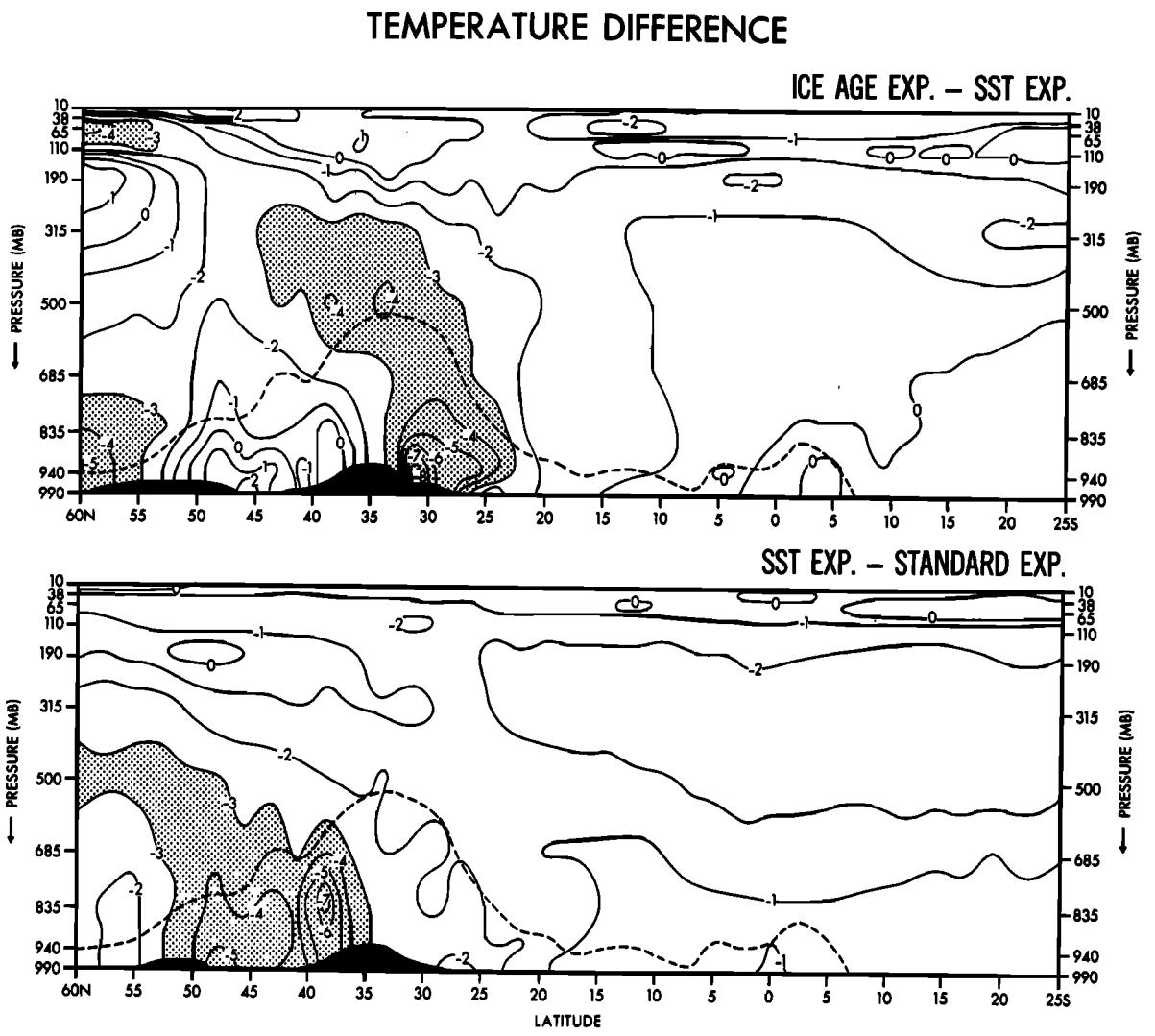

Fig. 26. Latitude-pressure distributions of temperature difference (in degrees Celsius) averaged over the longitudinal range 55°-105°E: (top) ice age experiment – SST experiment and (bottom) SST experiment – standard experiment. The black region indicates the area of mountains present at all grid points within this longitudinal domain; dashed lines indicate the altitude of the highest mountains.

pressure over continents in the ice age experiment in light of hydrostatic considerations.

Figure 22*a* illustrates surface wind vectors and streamlines for the ice age and standard simulations. For ease of comparison the difference in surface wind vectors between the ice age and standard simulations is shown in Figure 22*b*. The difference wind vectors in this figure point outward from the northern portion of South America and from the west coast of tropical Africa into the warm temperature anomaly located around 20°N in the Atlantic Ocean (Figure 2). Also, the difference wind vectors in Figure 22*b* indicate an outflow from the east coast of tropical Africa and the Indian subcontinent into the warm anomalies in the Indian Ocean. The outflows described above are consistent with the geographical distribution of pressure difference between the two simulations (Figure 20). For example, the pressure differences around 20°N in the Atlantic Ocean are more negative than the pressure differences over tropical Africa or the northernmost portions of South America.

To appreciate further how aridity of the tropical continents is maintained, it is desirable to examine differences in moisture transport between the ice age and standard simulations. Figure 23 illustrates the geographical distribution of the vector difference in moisture transport by the stationary component of the flow. (The transport vector is defined by $\int_0^{P_*} \bar{\mathbf{V}} \cdot \bar{r} \cdot dp/g$, where p is pressure, P_* is surface pressure, $\bar{\mathbf{V}}$ is the July-August mean horizontal component of the wind, $\bar{r}$ is the July-August mean mixing ratio of water vapor, and g is the acceleration of gravity.) This figure indicates outflows similar to those in the map of surface vector difference shown in Figure 22*b* (i.e., the outflows from northern portions of South America into the Atlantic Ocean and from equatorial east Africa and the Indian subcontinent into the Indian Ocean). In addition, it reveals southward outflow from west Africa (in the neighborhood of the Ivory Coast) into the Atlantic Ocean. Similar outflow is not as evident in the distribution of surface wind difference. According to a detailed analysis this moisture outflow is caused not by change in the near-surface wind but by the reduction in the moisture content of the southwest monsoon flow due to the influence of ice age boundary conditions. Moisture content of air is generally lower in the ice age simulation than in the standard simulation owing to the overall reduction of air temperature.

SST experiment. The preceding discussions imply that

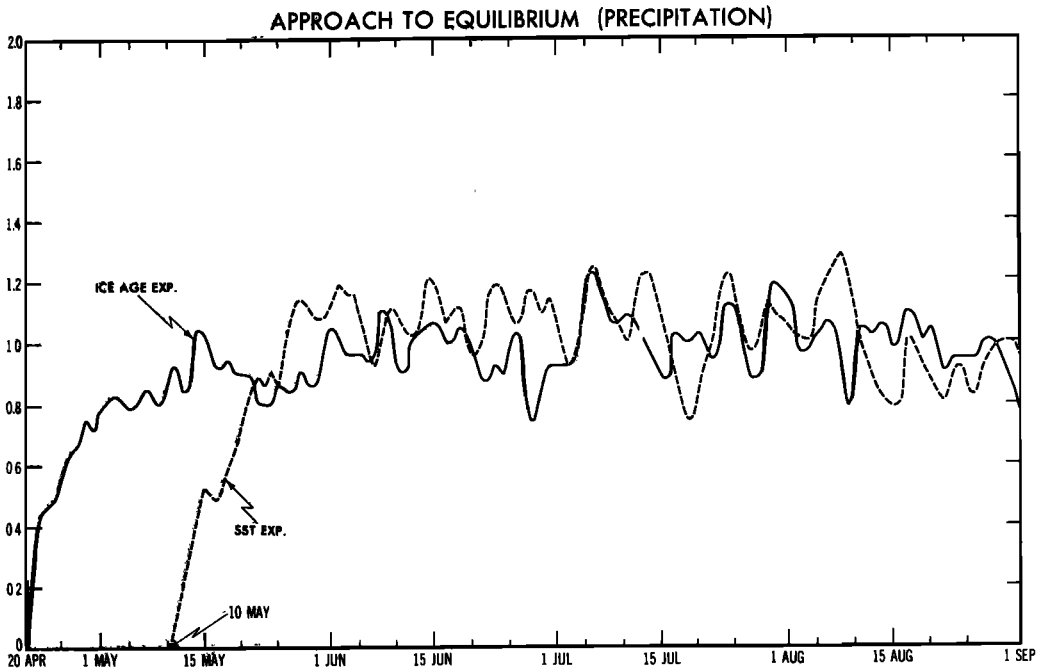

Fig. 27. Graphs of the quantity D with respect to time based on the time evolution of the precipitation distributions.

aridity of the continental tropics in the ice age simulation results not only from the relative warmth of ice age sea surface temperatures in low latitudes but also from the increase in surface albedo of the continental surface. In order to separate the climatic effects of the differences in sea surface temperature and surface albedo, it is desirable to examine the results from the SST experiment as well as from the two experiments discussed so far. For example, one can evaluate the climatic effects of the change in the sea surface temperature distribution by comparing results from the standard experiment with those from the SST experiment. The comparison between the SST and ice age experiments should yield insight into the climatic effect of changes in the condition of the continental surface, in particular, surface albedo. Here, it is important to note that the change in the condition of continental surface includes not only the increase of surface albedo but also the alterations of surface topography and continental outlines resulting from the growth of ice sheets. The influence of the latter changes, however, is thought to be small in low latitudes.

Figure 24 illustrates latitudinal distributions of zonal mean precipitation rate over continents from all three experiments. According to this figure the precipitation rate over tropical continents is largest in the standard simulation, substantially smaller in the SST simulation, and smallest in the ice age simulation. In other words, both the change in sea surface temperatures and the relatively high continental albedo values in the ice age experiment contribute significantly to the comparatively low precipitation rate over the tropical continents, although the contribution of the former appears to be larger than that of the latter in the vicinity of the continental tropical rain belt.

Over the Indian subcontinent, however, the effect of surface albedo increase appears to be more important. This becomes evident if one compares the surface flow distributions of all

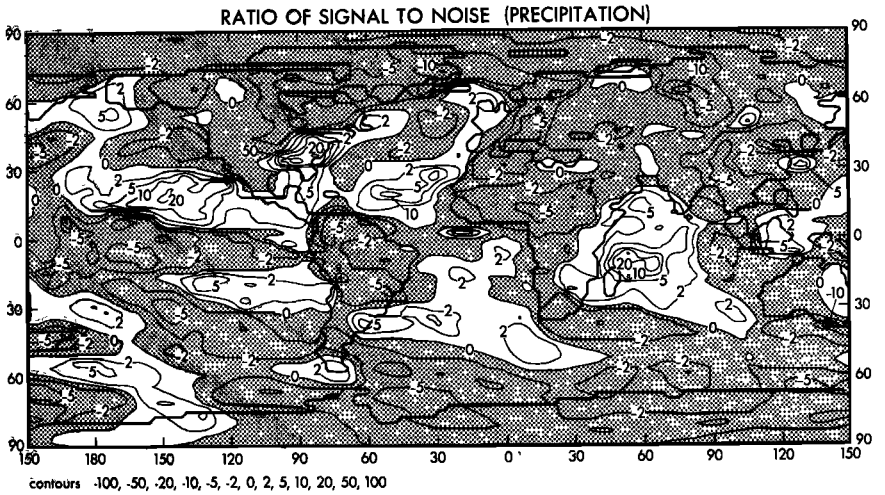

Fig. 28. Geographical distribution of the signal-to-noise ratio based on the rate of precipitation of the ice age and standard experiments.

TABLE 2. Area Integrals of Surface Temperature Differences (in Degrees Celsius) Which Compare Results From Standard, Ice Age, and SST Experiments

	Ice Age − Standard	Ice Age − SST	SST − Standard
	Land and Sea		
Northern hemisphere	−5.86 [−3.97]	−2.66 [−1.20]	−3.20 [−2.77]
Southern hemisphere	−4.90 [−2.78]	−0.20 [−0.49]	−4.70 [−2.29]
Global	−5.38 [−3.40]	−1.42 [−0.85]	−3.96 [−2.55]
	Land		
Northern hemisphere	−9.16 (−6.49)	−5.88 (3.56)	−3.28 (−2.93)
Southern hemisphere	−5.19 (−5.46)	−1.11 (−2.91)	−4.08 (−2.55)
Global	−7.69 (−6.19)	−4.17 (−3.37)	−3.52 (−2.82)
	Sea		
Northern hemisphere	−3.77 (−2.60)	−0.62 (0.00)	−3.15 (−2.60)
Southern hemisphere	−4.68 (−2.26)	+0.15 (0.00)	−4.83 (−2.26)
Global	−4.36 (−2.40)	−0.22 (0.00)	−4.14 (−2.40)

Values in brackets indicate integrals over ice-free points common to all three experiments; the ice-free grid point could be land in one and sea in another. Values in parentheses indicate integrals over points which are either land or sea and also ice free in all three experiments.

three experiments: Figures 22*a* and 25. These figures show that the southwesterlies extend all the way to the northern parts of India and Burma in both the standard and SST experiments, an indication that the change in sea surface temperature has little effect on the vigor and extent of the surface monsoon circulation. However, in the ice age experiment, southwesterly flow extends northward to the southern tip of the Indian peninsula, but it does not extend as far northward as it does in the other two experiments. In short, the increased albedo, rather than the change in sea surface temperature, is chiefly responsible for the weakness of the monsoon circulation in the ice age simulation. Weaker monsoon southwesterlies were noted by *Williams et al.* [1974] and *Gates* [1976*a*, *b*] in their ice age simulations.

In order to appreciate these results it is useful to examine the mass field in the neighborhood of the Indian subcontinent. Figure 26 illustrates latitude-pressure distributions of the difference in temperature between the ice age and SST simulations and the SST and standard simulations over the longitude belt from 55° to 105°E. Over and to the south of the Himalayas this figure indicates that the temperature difference between the ice age and SST simulations is much larger than the corresponding difference between the SST and standard simulations. In other words, the increase in the albedo of the continental surface is mainly responsible for reducing moist convective activity and, accordingly, tropospheric temperatures over and to the south of the Himalayas in the ice age experiment. The lower temperatures hydrostatically produce higher sea level pressures (see Figure 19), which in turn prevent the penetration of southwesterlies northward beyond the southern portions of India and Burma. This result is not inconsistent with the results of *Walker* [1910] and *Hahn and Shukla* [1976], which show that the extent of snow cover over Asia in winter is negatively correlated with the amount of monsoon precipitation over India in the following summer.

Conclusion

It is shown that the climate over tropical continents is much dryer in the ice age simulation than in the standard simulation, a finding in agreement with recent geological evidence. Although the period of analysis is limited to only the July-August season, the results appear to yield some insight on how aridity of the continental tropics is maintained.

According to comparisons between the ice age and standard simulations, tropical continental aridity of the ice age results from stronger surface outflow from continents (or weaker surface inflow from oceans). The stronger outflow enhances sinking (or weakens rising motion) and thus reduces rainfall over tropical continents.

The difference between the ice age and modern distributions of sea surface temperature is particularly large in high latitudes but is small in the tropical oceans at both sides of the equator, where zonally elongated zones of minimum temperature dif-

TABLE 3. Area Integrals of Rate of Precipitation (in Centimeters per Day)

	Standard	Ice Age	SST
	Land and Sea		
Northern hemisphere	0.351 (1.00)	0.325 (0.93)	0.344 (0.98)
Southern hemisphere	0.236 (1.00)	0.203 (0.86)	0.199 (0.84)
Global	0.293 (1.00)	0.264 (0.90)	0.272 (0.93)
	Land		
Northern hemisphere	0.332 (1.00)	0.229 (0.69)	0.292 (0.88)
Southern hemisphere	0.156 (1.00)	0.109 (0.70)	0.146 (0.94)
Global	0.274 (1.00)	0.190 (0.69)	0.244 (0.89)
	Sea		
Northern hemisphere	0.363 (1.00)	0.396 (1.09)	0.378 (1.04)
Southern hemisphere	0.255 (1.00)	0.226 (0.89)	0.212 (0.83)
Global	0.302 (1.00)	0.298 (0.99)	0.283 (0.94)

Values in parentheses indicate rate of precipitation scaled by that of the standard experiment.

ference are located. In these regions, one can identify so-called warm anomalies, where sea surface temperatures during the ice age are comparable with present temperatures despite the coldness of the surrounding sea surface. Because of the increased temperature contrast with the surroundings these warm anomalies enhance evaporation, moist convection, precipitation, release of latent heat, and the development of warm core tropical cyclones, which in turn contribute to reduce the time mean sea level pressure and intensify general upward motion. Over continents, surface albedo of the ice age tends to be higher than that of the present because of the extensive ice sheets, snow, and meager vegetation. Accordingly, in the ice age experiment, tropospheric temperatures tend to be relatively low, and sea level pressures tend to be relatively high in comparison to oceanic values. Although some warm anomalies appear at the surface of tropical continents owing to dryness of the soil surface, they are not as effective in enhancing moist convection and releasing latent heat as their oceanic counterparts because of the lack of heat capacity and an insufficient supply of moisture. Therefore in response to ice age boundary conditions a land-to-sea surface pressure gradient develops which enhances outflow from continents (or reduces inflow from oceans) and contributes to the aridity of tropical continents in the ice age simulation.

It appears to be significant that in general, warm anomalies to the south of the equator are much less effective in enhancing moist convection and precipitation. This is because the warm anomalies in the southern hemisphere are located in the region where sea surface temperatures are substantially below tropical values and where the tropospheric air is very dry owing to adiabatic heating in the downward branch of the Hadley circulation.

In apparent agreement with speculation or the hypothesis of a pluvial tropical climate the southern (main) Hadley cell does intensify in response to ice age boundary conditions. However, this intensification is essentially a manifestation of the increase in the meridional circulation over the oceans. Over continental portions of the model tropics the vertical velocity in the upward-moving branch of the Hadley cell is much weaker in the ice age simulation, partly because of the near-surface convergence of continental air into oceanic rain belts. This result is consistent with the aridity in the continental tropics.

In conclusion, comparisons of results from the three numerical experiments suggest that surface temperature anomalies of tropical oceans affect the precipitation rate not only over oceans but also over continents. In addition, they suggest that a generally high albedo of the continental surface lowers atmospheric temperature, increases sea level pressure over continents, and has a profound effect on monsoon circulations in the tropics. For example, it is shown that the strength of south Asian summer monsoon circulation in the ice age experiment is significantly weaker than the intensity in the standard experiment mainly because of the increase of surface albedo over the Eurasian continent (in particular, over the Tibetan Plateau). One can speculate that some of the anomalies in the modern climate may be caused by similar mechanisms.

In this paper, no attempt has been made to identify the basic cause of an ice age. Also, it is not clear why the difference between present and ice age sea surface temperatures is so small at both sides of the equator. To investigate this question, it is necessary to use a climate model in which the influence of the ocean circulation is explicitly incorporated. However, one can speculate that ice age surface temperatures were indeed reduced more over land than over oceans. As has been discussed in this study, larger values of continental surface albedo obviously contribute to a greater reduction in land temperatures. Furthermore, surface temperature reduction, in response to a given increase in surface albedo, is larger over continents than over oceans, where larger proportions of available radiation energy are used for evaporation rather than for sensible heating.

It is important to keep in mind that the conclusions obtained in this study are based on several model assumptions, simplifications, and limitations. For example, improvement in model resolution or convective parameterization may alter some results. In particular, the incorporation of a cloud prediction scheme which is coupled to radiation computations may significantly change some conclusions.

APPENDIX 1. ADJUSTMENT TO NEW BOUNDARY CONDITIONS

For each control experiment (the ice age experiment and the SST experiment) which branches off from the standard experiment, it is necessary to ascertain that its time integration extends long enough that the control model atmosphere has sufficient time to adjust to its new boundary conditions. In order to show that these control experiments have reached such a quasi-equilibrium state, a quantity D which indicates a difference between the control and standard experiments is computed as follows:

$$D = \alpha_0^{-1} \int \alpha \, dA$$

where

$$\alpha = \text{sgn}\,(q_c^t - q_s^t) \cdot (q_c - q_s)$$

q represents any variable defined at a model grid point; c and s indicate variables taken from the control and standard experiments; t indicates a time average taken over the entire period of overlapped time integration, sgn ( ) indicates the algebraic sign of ( ); $\int$ ( ) dA denotes integration over the entire global domain; and α_0 is the time average of α over the last 2 months of the time integrations.

Figure 27 shows how the quantity D, defined above, changes with respect to time for the two control experiments. Since comparisons between various hydrologic quantities are discussed in detail throughout this paper, the quantity D is evaluated by using the precipitation rate as computed at each model grid point. As one can expect, D is zero when the time integration of a control experiment begins or branches off from the standard experiment, and it increases rapidly during the early stages of the integration. This figure indicates that the hydrologic cycle adjusts to the new boundary conditions for both experiments in less than 1 month and that quasi-steady states are achieved in the SST and ice age experiments long before July 1, the first day used for creating the 2-month time-averaged fields which are presented for comparison throughout this paper.

In addition, the quantity D is evaluated by using fields of sea level pressure. Similarly, although the figure is not shown here, it is concluded that the sea level pressure fields of the two control experiments reach a quasi-steady state in about 1 month.

APPENDIX 2. SIGNAL-TO-NOISE RATIO

It has been pointed out by *Leith* [1973] that in numerical experimentation studies in which we are interested in detecting the influence of external changes, such as sea surface temperature or solar constant, we must be able to distinguish between

the 'signal,' i.e., the change in the two climatic means, and the 'noise,' i.e., the natural fluctuation in the finite time mean state. To be able to claim that the differences between the two experiments are genuine and significant, we must take the average over longer periods, and this averaging period should be decided on the basis of analysis of variance of the time series of variables describing the model states.

Following Leith, for a random time series $\psi(t)$ with mean μ and standard deviation σ the error $\bar{\phi}(t)$ in estimating the mean due to averaging over a limited period T is given by

$$\bar{\psi}(t) = \mu + \bar{\phi}(t)$$

where

$$\overline{(\ )} = \frac{1}{T}\int_{-T/2}^{T/2}(\ )\,dt \qquad \psi(t) = \mu + \phi(t)$$

Here

$$\langle\phi(t)\rangle = 0 \qquad \langle\phi(t)\phi(t+\tau)\rangle = \sigma^2 R(\tau)$$

where the angle brackets denote the ensemble average and $R(\tau)$ is the correlation at lag time τ. The variance of $\bar{\phi}(t)$ may be given as

$$\langle\bar{\phi}(t)\bar{\phi}(t)\rangle = \sigma_T^2 = \frac{2\sigma^2}{T}\int_0^T\left(1 - \frac{\tau}{T}\right)R(\tau)\,d\tau$$

In Leith's analysis, σ_T is referred to as noise, and the difference between the means of the two model states, i.e., $\Delta\mu = (\mu_2 - \mu_1)$, is referred to as signal. For a result to be significant the signal-to-noise ratio must be greater than 1.

Again, the field of rate of precipitation is used for computing the signal-to-noise ratio, since various hydrologic quantities are discussed in detail throughout this paper. The signal is obtained by subtracting the values of the standard experiment from those of the ice age experiment. This difference map of the 60-day mean precipitation rate is given in Figure 8*b*. In addition, we must make the aforementioned statistical analysis to see which of these changes are significant. To make this test, the noise level is evaluated at each grid point by using the time variation of daily precipitation during the last 92 days of the standard experiment. For this computation of σ_T, $R(\tau)$ is assumed to be zero for $31 \leq \tau \leq 60$ days, an assumption which may tend to overestimate noise. Before these computations are made, the original precipitation fields are smoothed to reduce the small-scale spacial variability of rainfall.

Figure 28 shows the horizontal distribution of results from the signal-to-noise ratio computation. From this display, one can judge the relative significance of various features of the precipitation difference field. According to this figure the reduction of the time mean precipitation rate over tropical Africa and the tropical portions of South America appears to be very significant. These results imply that aridity of the model tropics, which is extensively discussed in this paper, is a significant feature of the ice age simulation and is not a manifestation of the natural fluctuation of the model climate.

APPENDIX 3. AREA INTEGRALS OF KEY CLIMATIC VARIABLES

In order to show the global response to ice age boundary conditions and to facilitate comparison with results from other ice age simulation studies, global and hemispheric integrals of key climatic variables are presented here. Table 2 shows the area integrals of surface temperature difference, and Table 3 contains the area means of rate of precipitation from the simulation experiments discussed in this study.

For the earth as a whole the mean surface temperature difference between the ice age and standard simulations is −5.38°C. The corresponding value from *Gates* [1976*a*], who based his ice age boundary conditions on the same Climap input, is −4.9°C. In addition, the results of this study show a reduction of the global mean rate of precipitation in the ice age experiment to 90% of that in the standard experiment, in good agreement with the results of *Gates* [1976*a*], which show a reduction to 88% of that in his standard experiment.

Over oceanic regions which are not covered by sea ice the ice age surface temperatures are, on the average, 2.4°C lower than those of the standard experiment. On the other hand, the corresponding reduction of surface temperature over the ice-free continental regions is about 6.2°C, a reduction much larger than the oceanic value. According to comparisons among the three experiments (i.e., the ice age, standard, and SST experiments), 46% of the continental reduction (2.8°C) results from imposing the distribution of ice age sea surface temperature and sea ice, and the remaining 54% (3.4°C) results from changing other boundary conditions, in particular, the change which resulted in a general increase in surface albedo over continents. As was discussed in the body of the text, relatively lower temperatures over land tend to produce a land-sea gradient in sea level pressure, which in turn contributes to a tendency for stronger outflow of near-surface air from continental regions to oceanic regions in the tropics of the ice age experiment.

Over land in the ice age experiment the rate of precipitation was reduced to 69% of that in the standard experiment, while over oceans the mean precipitation rate was reduced by only 1%. This differential response between land and sea is consistent with the tendency for increased outflow of near-surface air from continental regions in the ice age experiment, as was discussed above. It is also interesting to note that over oceanic regions in the northern hemisphere, where the effect of land-sea contrast is greater, the mean rate of precipitation actually increased in response to ice age boundary conditions. In the southern hemisphere the effect of land-sea contrast is smaller and is not able to overcome the effect of reduced atmospheric temperature and moisture content, an 11% decrease in the mean rate of precipitation over oceanic areas thus resulting.

Acknowledgments. We wish to thank the members of Climap for furnishing us with their reconstructions of the surface boundary conditions at 18,000 yr B.P. Thanks are also due Michael Sarnthein for furnishing us with the sand dune distributions used in verification of the model results. It is a pleasure to acknowledge the wholehearted support of J. Smagorinsky, Director of the Geophysical Fluid Dynamics Laboratory. The authors wish to thank D. Daniel for his effective day-by-day management of the model integrations and L. Dimmick and E. Green for their help in preparation of the model analysis material. Finally, the assistance provided by P. Tunison and his staff and E. Thompson was indispensable in the preparation of this manuscript.

REFERENCES

Alyea, F. N., Numerical simulation of an ice age paleoclimate, *Pap. 193*, Dep. of Atmos. Sci., Colo. State Univ., Fort Collins, 1972.

Charlesworth, J. K., *The Quaternary Era*, vol. 2, p. 1112, Edward Arnold, London, 1957.

Climap Project Members, The surface of the ice-age earth, *Science, 191*, 1131–1138, 1976.

Darmuth, J. F., and R. W. Fairbridge, Equatorial Atlantic deep-sea arkosic sands and ice-age aridity in tropical South America, *Geol. Soc. Amer. Bull., 81*, 189–206, 1970.

Gates, W. L., Modeling the ice age climate, *Science, 191*, 1138–1144, 1976*a*.

Gates, W. L., The numerical simulation of ice-age climate with a global general circulation model, *J. Atmos. Sci., 33,* 1844–1873, 1976*b*.

Hahn, D. G., and S. Manabe, The role of mountains in the south Asian monsoon circulation, *J. Atmos. Sci., 32,* 1515–1541, 1975.

Hahn, D. G., and S. Manabe, Reply, *J. Atmos. Sci., 33,* 2258–2262, 1976.

Hahn, D. G., and J. Shukla, An apparent relationship between Eurasian snow cover and Indian monsoon rainfall, *J. Atmos. Sci., 33,* 2461–2462, 1976.

Holloway, J. L., Jr., and S. Manabe, Simulation of climatology by a global general circulation model, *Mon. Weather Rev., 99,* 335–370, 1971.

Kendall, R. L., An ecological history of the Lake Victoria basin, *Ecol. Monogr., 39,* 121–176, 1969.

Kurihara, Y., and J. L. Holloway, Jr., Numerical integration of a nine-level global primitive equations model formulated by the box method, *Mon. Weather Rev., 95,* 509–530, 1967.

Leith, C., The standard error of time-average estimates of climatic means, *J. Appl. Meteorol., 12,* 1066–1069, 1973.

Livingston, D. A., Speculations on the climate history of mankind, *Amer. Sci., 59,* 332–337, 1971.

Manabe, S., Climate and the ocean circulation, 1, The atmospheric circulation and hydrology of the earth's surface, *Mon. Weather Rev., 97,* 749–774, 1969*a*.

Manabe, S., Climate and the ocean circulation, 2, The atmospheric circulation and the effects of heat transfer by ocean currents, *Mon. Weather Rev., 97,* 775–805, 1969*b*.

Manabe, S., and J. L. Holloway, Jr., The seasonal variation of the hydrologic cycle as simulated by a global model of the atmosphere, *J. Geophys. Res., 80,* 1617–1649, 1975.

Manabe, S., and J. D. Mahlman, Simulation of seasonal and interhemispheric variations in the stratospheric circulation, *J. Atmos. Sci., 33,* 2185–2217, 1976.

Manabe, S., and R. F. Strickler, Thermal equilibrium of the atmosphere with a convective adjustment, *J. Atmos. Sci., 21,* 361–385, 1964.

Manabe, S., and R. T. Wetherald, Thermal equilibrium of the atmosphere with a given distribution of relative humidity, *J. Atmos. Sci., 24,* 241–259, 1967.

Manabe, S., J. Smagorinsky, and R. F. Strickler, Simulated climatology of a general circulation model with a hydrologic cycle, *Mon. Weather Rev., 93,* 769–798, 1965.

Manabe, S., J. L. Holloway, Jr., and H. M. Stone, Tropical circulation in a time integration of a global model of the atmosphere, *J. Atmos. Sci., 27,* 580–613, 1970.

Manabe, S., D. G. Hahn, and J. L. Holloway, Jr., The seasonal variation of the tropical circulation as simulated by a global model of the atmosphere, *J. Atmos. Sci., 31,* 43–83, 1974.

Phillips, N. A., A coordinate system having some special advantage for numerical forecasting, *J. Meteorol., 14,* 184–185, 1957.

Posey, J. W., and P. F. Clapp, Global distribution of normal surface albedo, *Geofis. Int., 4*(1), 33–84, 1964.

Saltzman, B., and A. D. Venekar, A solution for the northern hemisphere climatic zonation during a glacial maximum, *Quaternary Res., 5,* 307–320, 1975.

Sarnthein, M., and L. Diester-Haass, Eolian sand turbidites, *J. Sediment. Petrology,* in press, 1977.

Servant, M., Séquences continentales et variations climatiques: Evolution du Bassin du Tchadau Cénozoique Supérieur, Orstom, Paris, 1973.

Smagorinsky, J., General circulation experiments with primitive equations, 1, The basic experiment, *Mon. Weather Rev., 93,* 99–164, 1963.

Street, F. A., and A. T. Grove, Environmental and climatic implications of late Quaternary lake-level fluctuations in Africa, *Nature, 261,* 385–390, 1976.

U.S. Navy Hydrographic Office, World atlas of sea surface temperature, *Publ. 225,* with suppl., Washington, D. C., 1964.

Venekar, A. D., Long-period global variations of incoming solar radiation, *Meteorol. Monogr., 12*(34), 1–21, 1972.

Walker, G. R., Correlations in seasonal variations of weather, 2, *Mem. Indian Meteorol. Dep., 21,* 22–45, 1910.

Williams, J., Simulations of the atmospheric circulation using the NCAR global circulation model with present day and glacial period boundary conditions, *Thesis 31,* Nat. Center for Atmos. Res., Univ. of Colo., Boulder, 1974.

Williams, M. A. J., Late Pleistocene tropical aridity synchronous in both hemispheres?, *Nature, 253,* 617–618, 1975.

Williams, J., R. G. Barry, and W. M. Washington, Simulation of the atmospheric circulation using the NCAR global circulation model with ice age boundary conditions, *J. Appl. Meteorol., 13,* 305–317, 1974.

(Received January 6, 1977;
revised April 13, 1977;
accepted April 26, 1977.)